

# A CHEMICAL PERCOLATION MODEL FOR DEVOLATILIZATION: SUMMARY<sup>†</sup>

**Thomas H. Fletcher\*** and **Alan R. Kerstein**  
*Combustion Research Facility, Sandia National Laboratories*  
*Livermore, California 94551-0969*

**Ronald J. Pugmire,\*\*** **Mark Solum,††** and **David M. Grant††**  
*Departments of Fuels Engineering\*\* and Chemistry††*  
*University of Utah, Salt Lake City, Utah 84112*

## Abstract

The chemical percolation devolatilization (CPD) model describes the devolatilization behavior of rapidly heated coal based on the chemical structure of the parent coal. This document provides complete details of the development of the CPD model. Percolation lattice statistics are employed to describe the generation of tar precursors of finite size based on the number of cleaved labile bonds in the infinite coal lattice. The chemical percolation devolatilization model described here includes treatment of vapor-liquid equilibrium and a crosslinking mechanism. The crosslinking mechanism permits reattachment of metaplast to the infinite char matrix. A generalized vapor pressure correlation for high molecular weight hydrocarbons, such as coal tar, is proposed based on data from coal liquids. Coal-independent kinetic parameters are employed. Coal-dependent chemical structure coefficients for the CPD model are taken directly from <sup>13</sup>C NMR measurements, with the exception of one empirical parameter representing the population of char bridges in the parent coal. This is in contrast to the previous and common practice of adjusting input coefficients to precisely match measured tar and total volatiles yields.

The CPD model successfully predicts the effects of pressure on tar and total volatiles yields observed in heated grid experiments for both bituminous coal and for lignite. Predictions of the amount and characteristics of gas and tar from many different coals compare well available data, which is unique because the majority of model input coefficients are taken directly from NMR data, rather than used as empirical fitting coefficients. Predicted tar molecular weights are consistent with size-exclusion chromatography (SEC) data and field ionization mass spectrometry (FIMS) data. Predictions of average molecular weights of aromatic clusters as a function of coal type agree with corresponding data from NMR analyses of parent coals. The direct use of chemical structure data as a function of coal type helps justify the model on a mechanistic rather than an empirical basis.

---

<sup>†</sup> Work supported by the U. S. Department of Energy's Pittsburgh Energy Technology Center's Direct Utilization AR&TD Program, the DOE Division of Engineering and Geosciences through the Office of Basic Energy Sciences, and by the National Science Foundation through the Advanced Combustion Engineering Research Center (ACERC) at Brigham Young University and the University of Utah.

\* Author to whom correspondence should be addressed. Presently at the Department of Chemical Engineering, 350 CB, Brigham Young University, Provo, Utah, 84602.

## I. Introduction

**a. Current Devolatilization Models.** It is generally agreed that the chemical diversity of various coals will affect their rates of combustion through the devolatilization process.<sup>1</sup> Upon heating, the labile chemical bonds in coal undergo cleavage resulting in the release of light gases and heavier molecular fragments that either vaporize as tars or remain the coal lattice as metaplast. Simultaneously, a fraction of the original coal is converted to char. The process by which the volatile components (light gases and tars) leave the solid coal particle as it is transformed into char is also an important step in coal devolatilization. Thus, both chemical and transport submodels in coal devolatilization become necessary components in any general description of coal combustion. It is of critical importance, however that such submodels be both computationally efficient and capable of incorporating analytical data characterizing the chemical structure of coals.

Models of coal devolatilization have progressed from simple empirical expressions of total mass release, involving one or two rate expressions, to more complex descriptions of the chemical and physical processes involved. Reviews of these processes, occurring during coal pyrolysis, have been published by several investigators.<sup>1-6</sup> During coal pyrolysis, the labile bonds between the aromatic clusters are cleaved, generating fragments of finite molecular weight. Fragments with low molecular weights vaporize due to their high vapor pressure and escape from the coal particle as tar vapor. The fragments with high molecular weight, and hence low vapor pressures, tend to reside in the coal under typical devolatilization conditions until they reattach to the lattice. These high molecular weight compounds plus the residual lattice are referred to as metaplast. The quantity and nature of the metaplast generated during devolatilization, as well as subsequent crosslinking reactions, determines the softening behavior of the particle.

The relationship between the number of labile bonds broken and the mass of finite fragments liberated from the infinite coal lattice is highly non-linear, indicating that coal pyrolysis is not a simple vaporization process. Freihaut and Proscia<sup>7</sup> collected coal tars from a heated screen reactor, and then measured the temperature at which these tars would revaporize in a subsequent experiment at identical heating conditions. The coal tars revaporized at significantly lower temperatures than the original temperature of tar release from the coal. These results demonstrate that coal pyrolysis is not just a vaporization process, and suggest that lattice networks may be necessary to describe coal pyrolysis reactions.

The concept of breaking bonds with a variety of activation energies was first addressed by Pitt,<sup>8</sup> who treated coal as a collection of a large number of species decomposing by parallel first order reactions. A similar concept was employed by Anthony et. al.<sup>9</sup> and Anthony and Howard<sup>10</sup> to give the Distributed Activation Energy Model (DAEM). Kobayashi, et al.<sup>11</sup> introduced a chemical diversity into devolatilization with a set of two competing reactions, allowing preferential char formation at lower temperatures. The tabulation by Gavalas<sup>1</sup> of energies for a large variety of chemical bonds lends support to the concept that the bond breaking process is governed by a distribution of bond types in typical coals. The use of an average activation energy with a spread of energies, designated by a standard deviation and a corresponding Gaussian distribution, provides an alternative to the use of a large set of differential equations which might otherwise over-parameterize the description of the bond breaking process relative to the amount of reliable experimental data presently available on tar formation.

The distributed-energy chain statistics (DISCHAIN) model<sup>12-14</sup> of devolatilization uses string statistics to predict the production of monomer species, which play a dual role as a source of volatile tar and as a reactant which could polymerize at chain ends to form char. Niksa<sup>15</sup> originally used a gamma distribution function as a means to introduce a molecular weight distribution for tar yields into a new flash distillation model of devolatilization. This model also introduces a mechanism to treat tar vaporization as a multicomponent vapor-liquid equilibrium process. Arguments were presented to show that diffusion of the volatile species within the metaplast does not significantly affect pyrolysis behavior. The flash distillation mechanism was recently incorporated into the DISCHAIN model and named FLASHCHAIN.<sup>16</sup> In FLASHCHAIN, population balances are used to account for the distribution of mass in each molecular weight size bin based on the chain statistics, the flash distillation process, and a crosslinking mechanism. The population balance approach is almost as time-consuming as the Monte Carlo approach, and would require specification of the rates of reaction of each fragment size in a totally general case. Niksa assumed that these rates of reaction were all identical. The FLASHCHAIN model has been shown to compare well with a wide variety of experimental data, although the vapor pressure coefficients are determined empirically and do not correspond well with independent vapor pressure data. Some chemical structure data is used in FLASHCHAIN, although the coordination number is set to 2 in the chain formulation, and bridge molecular weights in the model are higher than the molecular weights of the aromatic portion of the clusters.

A detailed chemical model for the release of both tar and light gases during devolatilization has been discussed by Solomon and coworkers.<sup>5,17</sup> Nineteen first-order, distributed-energy rate expressions for the release of various light gases have been provided by these investigators, and their set of differential equations may be used to augment all lattice models of coal devolatilization. It is impractical, however, to extend this kind of comprehensive approach for gas release to the production of tar with its very large number of unique molecular species. Thus, Solomon and coworkers<sup>5,17</sup> characterized tar production with a single first-order, distributed-energy rate expression with chain statistics<sup>17b-c</sup> and with lattice statistics.<sup>17a,17d-f,18</sup> Bautista et al.<sup>19</sup> also have emphasized the importance of chemistry in devolatilization by discussing some of the important connections between char and tar formation and of the various gas release mechanisms for low CO<sub>2</sub> producing coals.

A desirable feature for any devolatilization model would be the prediction of molecular weight distributions now available for tars from the work of Solomon and coworkers,<sup>18</sup> Suuberg et al.<sup>20</sup> and Freihaut and coworkers.<sup>21</sup> The Suuberg data include not only the volatile fractions with a lower average molecular weight but also the heavier extractables remaining in the char fraction.

**b. NMR Chemical Analysis.** In order to incorporate chemical factors readily into a coal devolatilization model, it is important that the model be formulated in such a manner that chemical analytical data may be used as input parameters in the differential equations governing the devolatilization processes. A large number of chemical analytical techniques, now available for characterization of coal structure, are described by Karr<sup>22</sup> and include Fourier transform infra-red (FTIR),<sup>17</sup> pyrolysis mass spectroscopy,<sup>23</sup> and solid state nuclear magnetic resonance (NMR).<sup>24-26</sup> Particularly useful is the CP/MAS (cross polarization/magic angle spinning) method<sup>27-31</sup> in solid state NMR which provides a capability for characterizing directly the relative number of carbon

atoms in a variety of bonding configurations. The data should be acquired using the extrapolation techniques of Solum et al.<sup>31</sup> in order to obtain data on the various structural types of carbons in coal. The relative numbers of hydrogen and oxygen atoms is obtained from elemental analysis and structural features inferred indirectly from the NMR data.

Using solid state NMR methods to determine the compositions of various chemical moieties within coals provides some of the chemical information needed in the CPD devolatilization model. For example, the ratio of aromatic bridge-head carbons to total aromatic carbons provides a functional measure of the number of aromatic carbon atoms in a typical cluster of fused aromatic rings.<sup>31-33</sup> These data, along with the number of peripheral carbon atoms per cluster involved in side chains or bridges, provide rough estimates of the average molecular weight of a cluster, and of the number of branching sites for the cluster. Both of these quantities are important measures for characterizing lattice statistics<sup>33</sup> and guide the selection of some input parameters in the chemical devolatilization model. Thus, NMR data have become an important component in the development of a chemically based devolatilization model.

**c. Lattice Statistics.** The importance of lattice statistics in coal devolatilization for modeling both labile bond cleavage and char bond forming processes was exhibited originally by Solomon and coworkers<sup>18</sup> using Monte Carlo simulations. Their work on pyrolysis has shown that many of the mechanistic features of the time-dependent conversion of the coal macromolecule into molecular fragments depend upon lattice statistics. Use of percolation theory to provide analytical expressions for the statistics of bridge dissociations involved in devolatilization avoids the time consuming Monte Carlo techniques while preserving many of the significant statistical features of lattices. The use of percolation lattice statistics also eliminates some of the empiricism necessary in selecting input lattice configurations for the Monte Carlo method. The essential features of many problems (e.g. chemical polymerization, propagation of diseases and forest fires, flow of liquids through porous media, etc.) can be represented by the percolation statistics of lattice sites joined together with bridges. Statistics of real two and three dimensional arrays are not in general analytically tractable due to looping of sites and bridges within the lattice, but a class of pseudo lattices referred to as Bethe lattices have analytical solutions based on percolation theory.<sup>34,35</sup> These Bethe lattices are similar to standard lattices in that they may be characterized by a coordination number and a bridge population parameter, but differ from standard lattices in that any two sites in a pseudo lattice are connected only by a single path of bridges and sites. The presence of loops in standard lattices prevents the description of the lattice statistics in closed form, and it is such features which require the more extensive computational Monte Carlo method. The mathematical constructs of percolation theory, as applied to pseudo lattices, have been demonstrated repeatedly to represent the properties of real lattices whenever the average size of the finite fragments is modest.<sup>36-39</sup>

Percolation theory analytically describes the size distribution of finite clusters of sites joined by intact bridges but isolated from all remaining sites by broken bridges. Furthermore, the theory specifies a critical bridge population, depending only on the site coordination number, above which infinite arrays will coexist with fragments of finite size. It is a relatively simple matter to adapt the structural features of percolation theory to coals and their char and tar pairs obtained during pyrolysis. The infinite arrays of percolation theory are interpreted as macroscopic lattices of unreacted coal and/or char while relatively small tar molecules are identified with the finite

fragments of percolation theory. Kerstein and Niksa<sup>40,41</sup> used percolation theory to extend chain statistics (a Bethe lattice with coordination number of two) to higher coordination numbers in their DISCHAIN model. Although they didn't exploit the full potential of percolation theory for characterizing the distribution in molecular clusters of various sizes, their results provided some of the initial motivation for the theoretical developments which followed later. More recent work by Niksa and Kerstein<sup>16</sup> uses percolation chain statistics in connection with a population balance for fragments with low molecular weight.

**d. The Chemical Percolation Devolatilization (CPD) Model.** In this model, coal is visualized as a macromolecular array whose building blocks are clusters of fused aromatic rings of various sizes and types, including heteroaromatic systems with both nitrogen and oxygen atoms. These aromatic clusters are interconnected by a variety of chemical bridges, some of which are labile bonds that break readily during coal pyrolysis, while others are stable at a given temperature. The bridges which remain intact throughout a given thermal process are referred to as charred bridges. Obviously the definitions for labile and charred bridges are somewhat relative depending upon the pyrolysis temperature and the kinetic parameters appropriate for a given bridge. Side chain attachments to the aromatic clusters include aliphatic ( $-\text{CH}_n$ ) and carbonyl ( $-\text{CO}_2$ ) groups, which are light gas precursors. Detached fragments from the coal matrix consist of one or more aromatic clusters connected to each other by labile and/or char bridges. Hence, a cluster consists of several fused rings with associated attachments (see Sec. II d), while a fragment consists of several sets of interconnected clusters. A small fraction of the clusters in the parent coal are unattached to the infinite matrix, and can be extracted using suitable solvents without breaking any covalent bonds.

Several hypothetical chemical structures for coal macromolecules have been suggested;<sup>3,42-44</sup> a simplistic approach is used in this work, with broad definitions of clusters, bridges, side chains, and loops, as illustrated in Fig. 1. Coal pyrolysis products include light gases, tar (hydrocarbons that condense at room temperature and pressure), and char.

Distributed activation energies are utilized in this model, but this approach does not avoid completely the need to redefine the character of labile bridges whenever very different temperature regimes are considered. Literature values for the kinetic parameters are used whenever available in the CPD model. The model incorporates ultimate gas yields and chemical structural data from solid state NMR analyses to guide the selection of fixed input parameters. It is also important to validate the fitting parameters important in the kinetic differential equations which characterize the breaking and charring of chemical bridges. This model also exploits the desirable features of percolation theory for specifying the total yield and mass distribution of tar species for a given degree of bond rupture.

The approach used in this paper includes the following features: 1) chemically dependent input parameters, determined in part from NMR data, are used to reflect the chemical diversity found in coals of different rank and type. 2) Lattice statistics are implemented with explicit mathematical functions. 3) The distribution of tar molecular clusters of various sizes as well as the fraction of material in the infinite char array are provided directly by analytical expressions from percolation theory. 4) The activation energy obtained by Solomon<sup>5,17</sup> for tar release is used. 5) The average

activation energy and frequency factor for light gas release is obtained from a weighted average of the complete set of reaction parameters given by Solomon et al.<sup>5,17</sup> for the release of individual gas species. The number of rate equations for gas release can be increased without violating the restrictions of the CPD model, but this is not done in order to focus on the overall features of gas, tar and char production and their relationship to lattice statistics. A more complete gas release model<sup>5,17</sup> may be used to differentiate between the fully and incompletely oxidized light gases released in the devolatilization process. 6) A simplified method is used to calculate the distributed activation energies on both tar and light gas release.

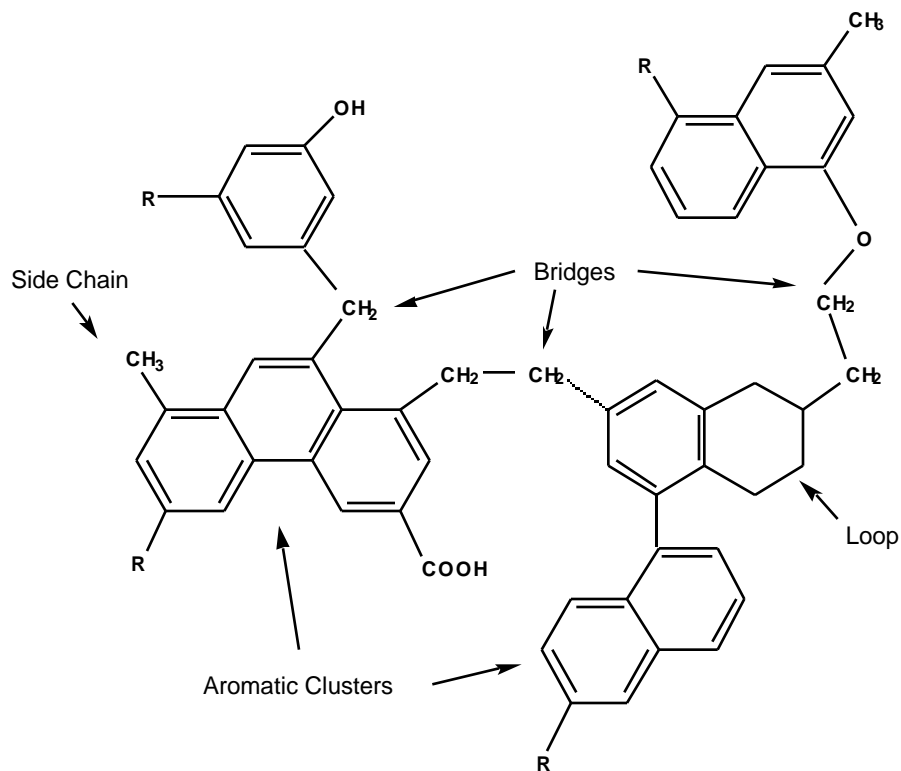


Figure 1. Representative chemical structures identified in  $^{13}\text{C}$  NMR analyses and used in the description of coal and coal chars in the CPD model.

The original CPD paper<sup>6</sup> demonstrated the ability of lattice statistics, coupled with a coal pyrolysis mechanism, to describe a set of data reported by Serio and coworkers<sup>5</sup> which was limited to a narrow range of heating rates and temperatures. A subsequent paper then explored the temperature dependence of the competition between the bridge scission rate (leading to tar formation) and the char bridge formation rate.<sup>45</sup> All of the fragments of finite size were assumed to be released as tar in early formulations of this model. Rate coefficients for the CPD model were obtained by comparison of model predictions with tar and total volatiles yield data from several coals of different rank over a wide range of temperature and heating rates at atmospheric pressure. Pressure-dependent devolatilization behavior was not addressed in the previous application of the CPD model, since a connection between vaporization and fragment molecular weight was not fully

developed. The present description of the CPD model exploits these features, permitting calculation of the molecular weight distribution of the finite fragments formed during bridge scission and the treatment of pressure effects. The addition of these features to the CPD model also permits direct use of chemical structure parameters of the parent coal, as measured by  $^{13}\text{C}$  NMR spectroscopy, without sacrificing agreement with experimentally-measured tar and total volatiles yields.

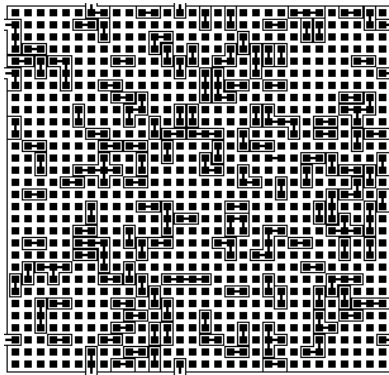
The CPD model treats the distinction between (a) low molecular weight aromatic fragments that vaporize as tar and (b) high molecular weight fragments that remain with the char in a liquid or solid state as metaplast. A new vapor pressure correlation was developed from data on coal liquids that allows predictions of tar molecular weights and yields as a function of residence time, temperature, and pressure. The correlation compares well with tabulated vapor pressure data for a wide variety of pure organic components. In contrast to previous efforts where model input parameters describing chemical structure are adjusted to force agreement between predicted and measured tar and total volatiles yields, coal-dependent chemical structure coefficients for the CPD model are taken directly from  $^{13}\text{C}$  NMR analyses of parent coals. This procedure eliminates most adjustable parameters from the model, and predictions of tar and total volatiles yields become true tests of the model and the NMR data, rather than mere results of curve-fitting. Resulting model predictions of tar and total volatiles yields as a function of coal type, temperature, heating rate, and pressure compare well with available experimental data, showing the value of both the model and the NMR chemical structure data.

## II. Lattice Statistics in Devolatilization

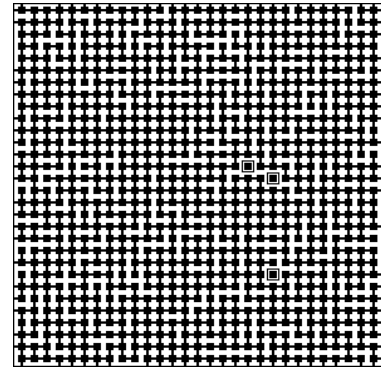
Before discussing the mathematical aspects of percolation theory used in the CPD model it is helpful to survey some of the statistical properties of lattices and their implications. Consider for various values of  $p$  (the fraction of intact bridges), the real, square two-dimensional lattice of coordination number 4 (four bridges attached to each lattice site) portrayed in Fig. 2. Monte Carlo methods\* are used to illustrate the sensitivity of cluster size on the ratio of intact to broken bridges in this two-dimensional square lattice. For a relatively low bridge population number,  $p$ , only fragments of finite size are observed. See Fig. 2a for  $p = 0.1$  where most of the fragments are monomers and not bridged to any other site. Nonetheless, there are a number of dimers, trimers, and other fragments or "mers" of larger size in this representation. Conversely, for  $p = 0.8$  (see Fig. 2b), only three monomer fragments are found in the representation containing 900 clusters with all of the remaining clusters belonging to the infinite array (i.e. every one of the remaining 897 clusters may be traced to each other through one or more paths in the lattice of bridges). Note, the use of the term infinite is appropriate as bridges at the border wrap around to the opposite side of the representation.

---

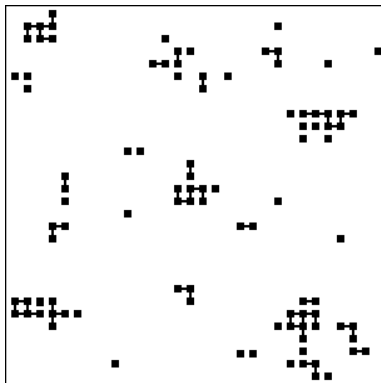
\* The random numbers generated in the Monte Carlo calculation were partitioned to approximate the value of  $p$ . Since a relatively small (30x30) realization is used to illustrate the principles under discussion, minor deviations from the idealized  $p$  may be encountered.



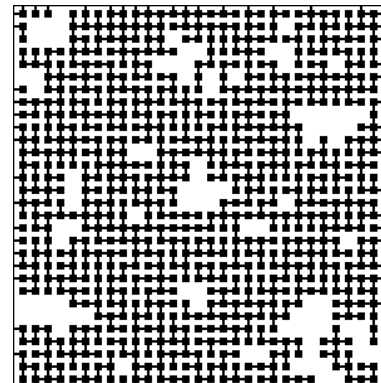
a.  $p = 0.1$



b.  $p = 0.8$



c.  $p = 0.55$ , finite fragments



d.  $p = 0.55$ , infinite lattice

Figure 2. Monte Carlo simulations of the square lattices with coordination number equal to 4 and for various bridge populations. In part a, only small fragments of small size are observed, while in part b all but three sites belong to the infinite array. For the bridge population of 0.55, finite fragments (c) and the infinite array (d) have been portrayed separately for clarity. For this value of  $p$ , only 11% of the sites are in finite fragments in this realization.

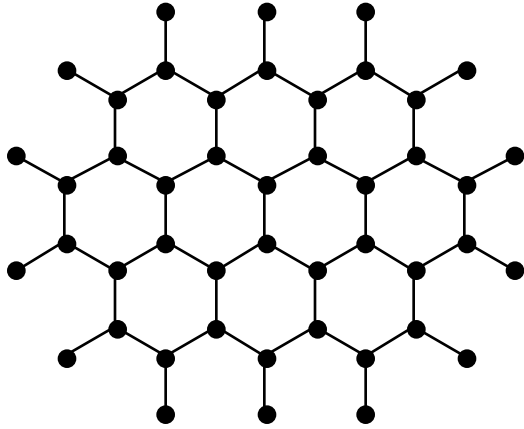
The point to be made is that over 99% of lattice sites are still connected even though 20% of the connecting bridges have been broken. For a value of  $p = 0.55$  (i.e. only 55% of the bridges are intact) the number of clusters in fragments of finite size is 11% of the total as shown in Fig. 2c, while the infinite array, Fig. 2d, contains 89% of the clusters. For the sake of clarity the finite fragments and the infinite array in the  $p = 0.55$  simulation are divided into two separate portrayals in Figs. 2c and 2d, respectively. Thus, Fig. 2 shows that the relationship between the fraction of finite fragments and the fraction of ruptured bridges in the lattice is highly non-linear.

The non-linear relationship between the distribution of finite fragments and the fraction of broken bridges is a significant feature of lattice statistics which has interesting implications in coal devolatilization. As the number of broken bridges increases, so will the fraction of finite fragments increase relative to the fraction of clusters connected to the infinite array. However, when  $p$  is in the range where the infinite array dominates, only monomers exist to any appreciable extent. Relative enrichment of the larger finite fragments is realized only as  $p$  decreases and approaches the critical point where the infinite arrays are finally consumed. Below this critical point the larger finite fragments degrade into smaller fragments with bridge breaking in accordance with normal intuition. Thus, above the critical point where the infinite array exists these statistics actually predict that the smaller finite fragments have a larger relative population as  $p$  approaches unity. At  $p$  equal to 1.0 it is, of course, impossible for any finite fragment to exist.

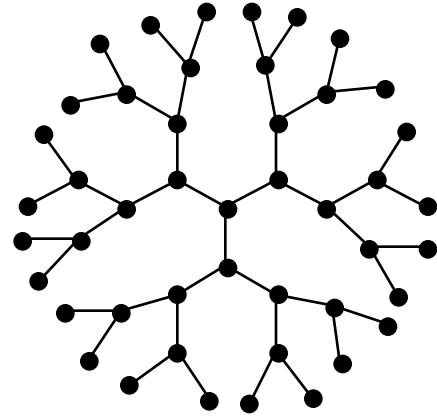
Monte Carlo simulations of bridge breaking are suitable for describing lattice features (assuming the realization is large enough), but they are computationally demanding. Percolation theory provides a computationally efficient way to simulate pyrolysis reactions for many particles involving numerical iterations in three dimensional grid arrays (e.g. in comprehensive coal combustion models<sup>46,47</sup>). Loops in real hydrocarbon lattices can link two or more sites through more than one pathway, and this feature of real lattices prevents one from obtaining simple analytical expressions for the essential statistical quantities characterizing these lattices. The use of Bethe pseudo lattices or trees, shown in Fig. 3 for two typical coordination numbers of 3 and 4, resolves this difficulty by removing the possibility of looping found, respectively, in the honeycomb and diamond real lattices, also given in Fig. 3.

The pseudo lattices have many properties that are similar to the corresponding real lattices for those problems in which only the smaller finite clusters and the infinite arrays are important. Only for clusters which become intermediate in size (e.g. hexamers and above) will the statistics of real and pseudo lattices differ appreciably. In such instances the percolation theory of pseudo lattices can differ from Monte Carlo calculations on real lattices of the same coordination number. Both approaches, however, predict very small populations for such intermediate size clusters except in the immediate vicinity of the critical point. Should a given property (e.g. higher order mass-weighted distributions) depend solely on those clusters of intermediate sizes, even though the overall concentration is very small, then the Bethe lattice representation could encounter difficulty.

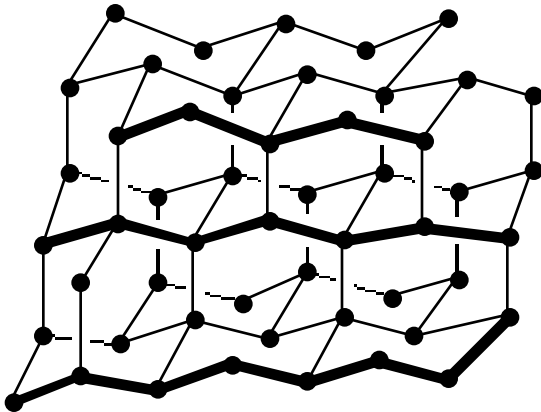
The formalism of Fisher and Essam<sup>35</sup> is followed closely in the mathematical development given in the Appendix, and this citation is the fundamental source for additional information on the statistics of Bethe lattices. The expressions used in this work are given for statistical quantities based on site counting, but the conversion between these expressions and the corresponding statistical expressions based on bridge counting is straightforward. For mathematical convenience, the



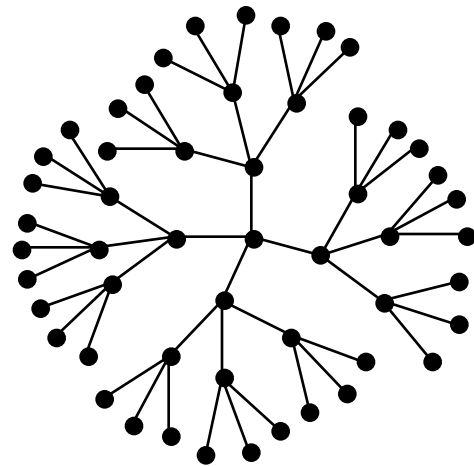
**HONEYCOMB LATTICE**



**TRIGONAL BETHE LATTICE**



**DIAMOND LATTICE**



**TETRAGONAL BETHE LATTICE**

Figure 3. Representative real lattices (honeycomb and diamond) and Bethe pseudolattices (trigonal and tetragonal) for coordination numbers 3 and 4, respectively. While real lattices may have bridges that link sites through a variety of loops, Bethe lattices connect any two sites only through a single pathway of bridges and sites, thereby eliminating the possibility of looping.

coordination number of a Bethe pseudo lattice is denoted by  $(z + 1)$ . Lattice evolution is characterized by a time-dependent fraction,  $p$ , of bridges which remain intact, the remaining fraction,  $(1 - p)$ , having been broken. If bridge scission events are statistically independent, then the probability,  $F_n$ , that a given site is a member of a cluster of  $n$  sites with  $s$  bridges becomes:

$$F_n(p) = nb_n p^s (1 - p) \quad (1)$$

where the values of  $s$  and  $n$  are given by:

$$s = (n - 1)z \quad \text{and} \quad n = n(z - 1) + 2 \quad (2)$$

and  $n$  is the number of broken bridges on the perimeter of an  $s$ -bridge cluster. The severed bridges serve to isolate the cluster from all other sites or clusters. Figure 4 illustrates the variations in  $s$  and  $n$  for a variety of clusters of various  $z$  and  $n$  values. As there are no loops within a Bethe lattice (hence its mathematical tractability), the number of bridges in a finite fragment will always be one less than the number of connected sites as may be observed readily in Fig. 4. The value of  $n$  giving the number of isolating broken bridges is less obvious, but is easily rationalized by consideration of Bethe trees connecting  $n$  sites with a coordination number of  $z + 1$ .

The quantity  $nb_n$  appearing in Eq. 1 is the number of distinct configurations possible for a cluster of size  $n$  containing a given site, and  $b_n$  is the same quantity expressed on a per site basis. The equation for  $nb_n$ , which is discussed in more detail in the Appendix, is:

$$nb_n = \frac{z+1}{s+1} \binom{s+1}{s} = \frac{z+1}{n+1} \binom{n+1}{n-1} \quad (3)$$

with the binomial coefficient given for real (non-integer) indices  $\mu$  and  $\nu$  by:

$$\binom{\nu}{\mu} = \frac{\Gamma(\nu+1)}{\Gamma(\mu+1)\Gamma(\nu-\mu+1)} \quad (4)$$

where  $\Gamma$  is the standard gamma function. Here, non-integers arise from fractional values for  $z + 1$ , which might be interpreted as average values for lattices with mixed coordination numbers. The use of Eq. 4 with Eq. 3 and Eq. 1 gives an analytical expression for the probability of finding a cluster of size  $n$  with a bridge population  $p$ .

The total fraction of sites,  $F(p)$ , contained in all of the finite clusters is:

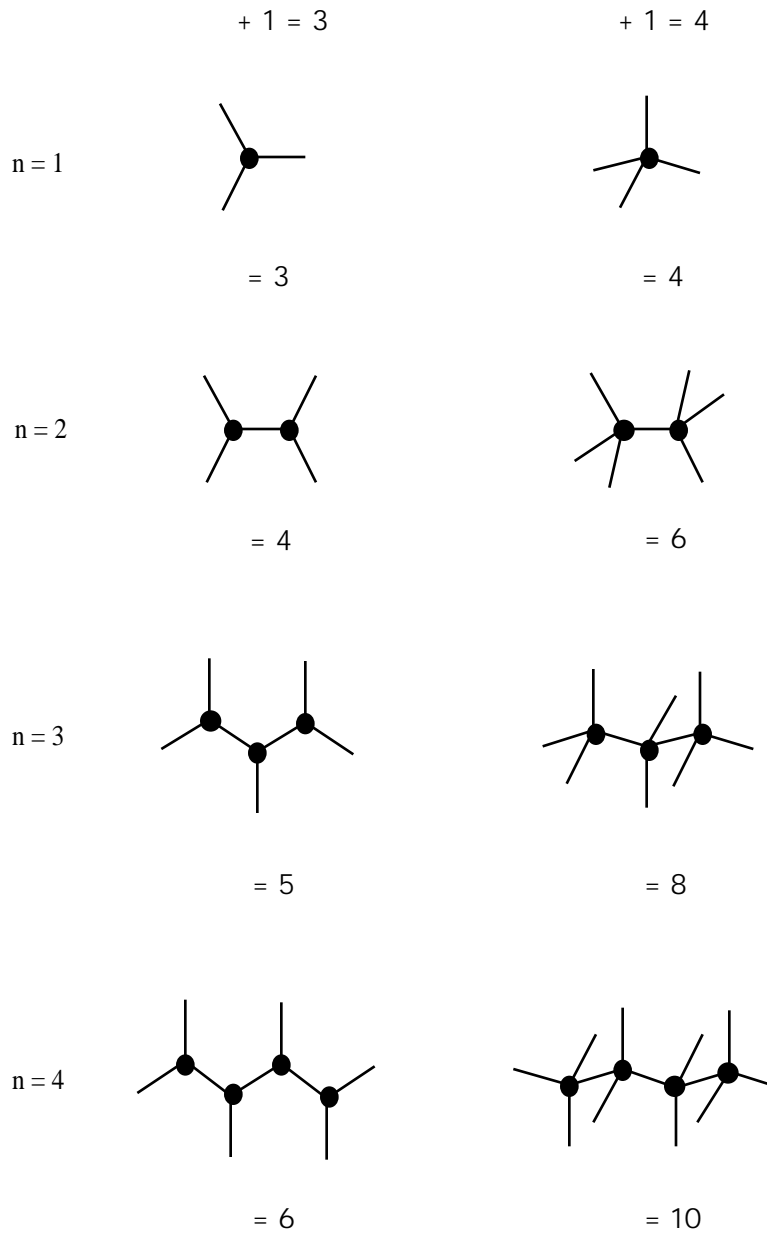


Figure 4. Representative fragments of various size  $n$  and coordination numbers ( $+1$ ) for a variety of fragment sizes (i.e., monomers, dimers, trimers, and tetramers). The value of  $\nu$  and its dependence on  $n$  and  $\nu$  is given for each of the clusters shown. The number of sites  $n$  is denoted by the filled circles. The number of isolating bridges  $\nu$  is given by line segments (representing broken bridges) attached to only one site and the number of bridges  $s$  is shown by line segments (representing bridges) connecting two sites.

$$F(p) = \sum_{n=1}^{\infty} F_n(p) = \left[ \frac{1-p}{1-p^*} \right]^{+1} = \left[ \frac{p^*}{p} \right]^{-\frac{+1}{-1}} \quad (5)$$

where  $p^*$  is the root of the following equation in  $p$

$$p^*(1-p^*)^{-1} = p(1-p)^{-1} \quad (6)$$

The value of  $p^*(1-p^*)^{-1}$  passes through a maximum at  $p = 1/2$ , the so-called percolation threshold or critical point. Below the critical point the appropriate solution of Eq. 6 is the trivial one of  $p^* = p$ . For  $p > 1/2$  the non-trivial solution of Eq. 6 may be used to evaluate the  $p^*$  needed in Eq. 5 to calculate  $F(p)$ . Conveniently, the appropriate root for  $p^*$  always falls in the range  $0 < p^* < 1/2$  for values of  $p$  both above and below the critical point, and these values are readily obtained from Eq. 6 using simple numerical methods. Above the percolation point the expression for  $F(p)$  given in Eq. 5 is no longer equal to 1, and the difference from unity is equal to the fraction of sites,  $R(p)$ , located in infinite arrays as follows:

$$R(p) = 1 - F(p) \quad (7)$$

A plot of  $F(p)$  versus  $p$  is given in Fig. 5 for several different values of  $(-1)$  to illustrate both the non-linear dependence of  $F(p)$  upon  $p$  and the inter-relationship of the several  $F(p)$  curves for different values of  $(-1)$ . The point at which  $F(p)$  drops sharply from unity is the so-called percolation threshold or critical point. Only in a very narrow range of  $p$  about this point will one find a significant number of larger finite fragments. Quantitative comparisons<sup>50</sup> of Bethe lattices and real lattices indicate good agreement with respect to the function  $F(p)$  providing that the respective lattices have the same percolation point.

The quantity  $F(p)$  is insufficient to characterize totally the tar yield, and requires two additional statistical quantities  $Q_n(p)$  and  $K(p)$  to account for the mass associated with the bridge and side chain fragments. They are:

$$Q_n(p) = F_n(p) / n = b_n p^{n-1} (1-p)^{n(-1)+2} \quad (8)$$

and

$$K(p) = \sum_{n=1}^{\infty} Q_n(p) = \left[ 1 - \left( \frac{+1}{2} \right) p^* \right] \left[ \frac{p^*}{p} \right]^{(+1)/(-1)} \quad (9)$$

where  $Q_n(p)$  is the number density of  $n$ -site clusters on a per site basis, and hence the reason for defining the configurational degeneracy factor in Eq. 1 as  $nb_n$ . The sum over  $Q_n(p)$  yields the configuration generating function  $K(p)$ . These terms are discussed further in the Appendix.

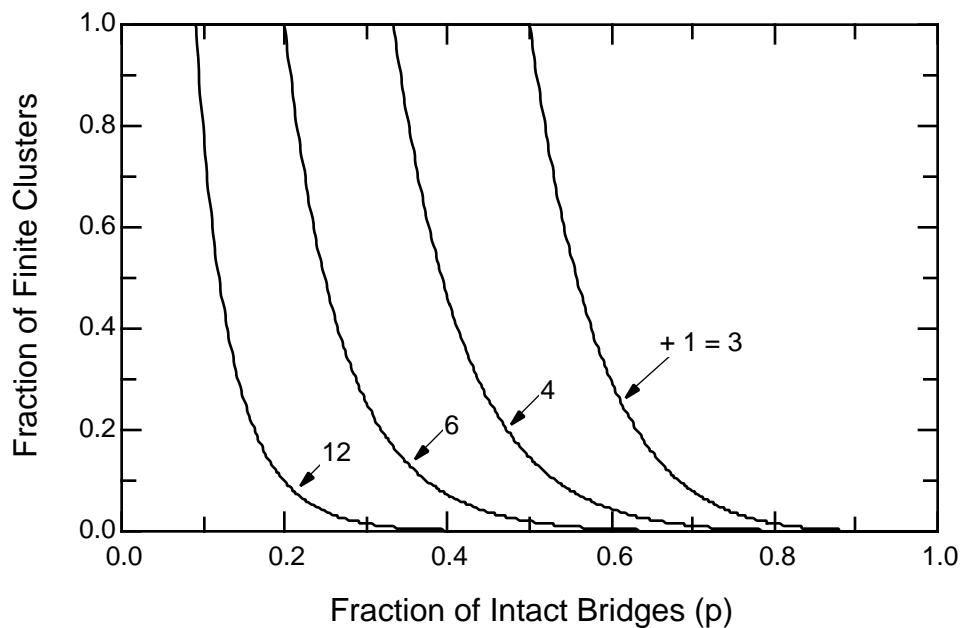
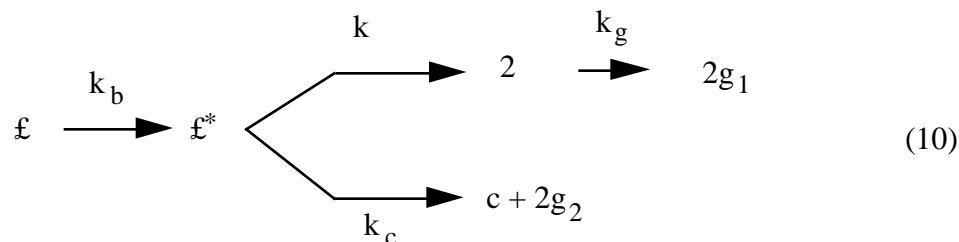


Figure 5. Value of  $F(p)$  giving the yield of finite fragments versus the bridge population,  $p$ , for representative coordination numbers,  $(z + 1) = 3, 4, 6,$  and  $12$ . The critical point at which the value of  $F(p)$  decreases from unity is given by  $1/z$ .

**a. Chemical Reaction Scheme.** The simple reaction sequence proposed in this work starts with (i) the breaking of a chemical bond in a labile bridge to form a highly reactive bridge intermediate (e.g. two free radical side chains temporarily trapped in the reaction cage) which is rapidly consumed by one of two competitive processes. The reactive bridge material either may be (ii) released as light gas with the concurrent relinking of the two associated sites within the reaction cage to give a stable or charred bridge, or else (iii) the bridge material may be stabilized (e.g. hydrogen extraction by the free radicals) to produce side chains from the reactive bridge fragments. These stabilized side chains may be (iv) converted eventually into light gas fragments through a subsequent, slower reaction. Thus, the following simple scheme is proposed to represent the devolatilization process:



A labile bridge, represented by  $\mathcal{L}$ , decomposes by a relatively slow step with rate constant  $k_b$  to form a reactive bridge intermediate,  $\mathcal{L}^*$ , which is unstable and reacts quickly in one of two

A labile bridge, represented by  $\mathcal{L}$ , decomposes by a relatively slow step with rate constant  $k_b$  to form a reactive bridge intermediate,  $\mathcal{L}^*$ , which is unstable and reacts quickly in one of two competitive reactions. In one reaction pathway, the reactive intermediate bridge  $\mathcal{L}^*$  is cleaved with rate constant  $k$ , and the two halves form side chains that remain attached to the respective aromatic clusters. Tar is generated as a sufficient number of bridges are cleaved to form finite fragments with sufficiently low molecular weight to vaporize. The side chains eventually undergo a cracking reaction to form light gas  $g_1$ . In a competing reaction pathway, the reactive intermediate  $\mathcal{L}^*$  is stabilized to form a stable "char" bridge  $c$  with the associated release of light gas  $g_2$  (rate constant  $k_c$ ). An illustrative example of the types of chemical transformations that may occur in this reaction scheme is given in Fig. 6. In this work, all mass connected to the infinite lattice is referred to as char, and is normalized by the initial amount of coal. Finite fragments that remain in the condensed phase are referred to as metaplast. At any instant the initial coal mass is divided into light gas, tar, metaplast, and char. From a chemical viewpoint, a portion of the material defined in this context as char includes any unreacted coal, as reflected in the fact that infinite lattices consist of labile bridges as well as stabilized char bridges during pyrolysis. The percolation statistics determine the populations of finite fragments (i.e., tar plus metaplast) as a function of the ratio of intact to broken bridges.

The competition for the reactive intermediate  $\mathcal{L}^*$  is governed by the ratio of the rate of side chain formation to the rate of char formation. The dynamic variables of the theory are the bridge population parameters,  $\mathcal{L}$  and  $c$ , and the side chain parameter  $\beta$ . The associated kinetic expressions for the proposed reaction mechanism (Eq. 10) are :

$$d\mathcal{L}/dt = -k_b \mathcal{L} \quad (11)$$

$$d\mathcal{L}^*/dt = k_b \mathcal{L} - (k + k_c) \mathcal{L}^* \quad (12)$$

where the symbols for the various species also represents their fractional abundance expressed as normalized bridge parameters. Using a steady state approximation for  $\mathcal{L}^*$ :

$$d\mathcal{L}^*/dt \approx 0 \quad \text{and thus} \quad \mathcal{L}^* \approx k_b \mathcal{L} / (k + k_c) \quad (13)$$

$$dc/dt = k_c \mathcal{L}^* \approx k_c k_b \mathcal{L} / (k + k_c) = k_b \mathcal{L} / (\beta + 1) \quad (14)$$

where  $\beta = k/k_c$ , and likewise:

$$\begin{aligned} d\beta/dt &= 2k \mathcal{L}^* - k_g \approx [2k k_b \mathcal{L} / (k + k_c)] - k_g \\ &= [2k_b \mathcal{L} / (\beta + 1)] - k_g \end{aligned} \quad (15)$$

$$dg_1/dt = k_g \quad (16)$$

$$dg_2/dt = 2 dc/dt \quad (17)$$

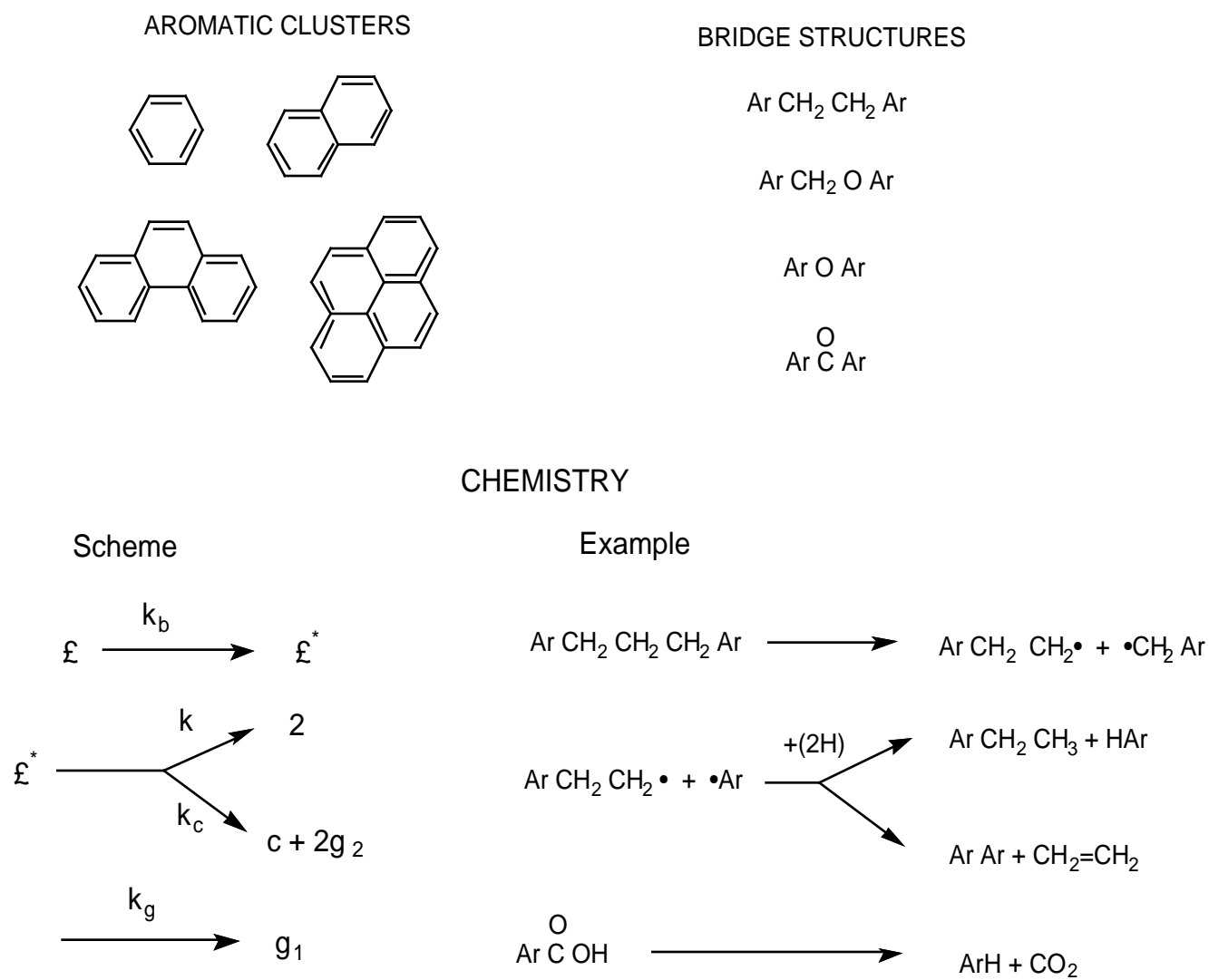


Figure 6. Representative chemical structures corresponding to the chemical reaction scheme in the CPD model.

The fraction of intact bridges,  $p$ , may be calculated from the bridge population parameters,  $\ell$  and  $c$ , as follows:

$$p = \ell + c \quad (18)$$

The fraction of broken bridges,  $f$ , is

$$f = 1 - p \quad (19)$$

In this formulation, it is easy to match the dynamic variables with the variables of percolation theory which depends upon the fraction of intact bridges,  $p$ , and the coordination number,  $z + 1$ . Percolation theory places no limits on the kinds of bridges which may be used to characterize the system providing they can be partitioned into either intact or broken bridges. In addition to the dynamic variables governing bridge populations, there are two gas dynamic variables,  $g_1$  and  $g_2$ , and a dynamic variable,  $g$ , to account for the metastable side chains. The variables  $g_1$ ,  $g_2$  and  $g$  are used to track the mass from the broken bridges and are written on a half bridge basis requiring a factor of two to relate them to the bridge population factors in a manner which is consistent with Eqs. 15-17.

**b. Mass Conservation and Initial Conditions** The following conservation of mass relationships constitute constraints on the dynamic variables:

$$g = g_1 + g_2 \quad (20)$$

$$g_1 = 2f - \ell \quad (21)$$

$$g_2 = 2(c - c_0) \quad (22)$$

The initial conditions for the dynamic variables of this system are given by:

$$c(0) = c_0 \quad (23)$$

$$\ell(0) = \ell_0 \quad (24)$$

$$g(0) = 2f_0 = 2(1 - c_0 - \ell_0) \quad (25)$$

$$g_1(0) = g_2(0) = 0 \quad (26)$$

Note that all initial conditions may be expressed in terms of the two parameters  $c_0$  and  $\ell_0$ .

**c. The Kinetic Reaction Parameters** The reaction rate equations for the bridge breaking and gas release steps are given in the Arrhenius form with a distributed activation energy as follows:

$$k_b = A_b \exp -[(E_b \pm V_b)/RT] \quad (27)$$

$$k_g = A_g \exp -[(E_g \pm V_g)/RT] \quad (28)$$

where the  $A_i$ ,  $E_i$  and  $V_i$  are, respectively, the pre-exponential frequency factor, the activation energy and the distributed variation in the activation energy for the  $i^{th}$  process. As the competitive processes depend only on the ratio of rate constants,  $= k / k_c$ , it is sufficient to write only one combined expression for these two steps as follows:

$$= k / k_c = A \exp -[(E \pm V)/RT] \quad (29)$$

where  $A = A / A_c$  and  $E = (E - E_c)$  and  $V$  is the corresponding distributed activation term.

**d. Light Gas, Tar and Char Weight Fractions** In the CPD model, bridge population parameters are normalized by the total number of bridges possible in the intact lattice. A terminology change from that used initially<sup>6</sup> has been made in order to clarify terms and to compare model results with additional NMR data. The term "sites" and "clusters" used by Grant, et al.<sup>6</sup> are now referred to in this work as "clusters" and "fragments," respectively. A site is defined as the fused ring portion of an aromatic cluster, whereas the term "cluster" is defined as the site plus any portion of the attachments which is not labile under bridge scission.

Finite fragments formed from bridge scission may consist of one aromatic cluster (monomer), two clusters connected by a labile or char bridge (dimer), or  $n$  clusters (fragment size  $n$ ) connected by  $n-1$  bridges. The bridge dynamic variables given in the above differential equations may be related now to the mass of the individual clusters and bridges. The total mass per cluster is:

$$m_{total}(t) = m_a + m_b (1 - c_0) ( + 1)/2 \quad (30)$$

where  $m_a$  is the average mass of the fused ring site and the second term on the RHS includes the mass of the bridges,  $m_b$ , corrected by the fraction  $(1 - c_0)$  for the fraction of bridges which might have already stabilized at time zero. The  $( + 1)/2$  term is the ratio of bridges to sites, and converts a bridge parameter such as  $(1 - c_0)$  into a per-cluster quantity. The mass of gas released up to time  $t$ , expressed on a per-cluster basis is:

$$m_{gas}(t) = m_b g ( + 1)/4 \quad (31)$$

The fraction of bridges which have been released as gas may be converted into a per-cluster variable by  $( + 1)/2$ , and an additional factor of  $1/2$  is inserted to convert  $m_b$  into the half bridge mass assigned to the average mass of side chains and of light gases released. The mass of a finite fragment of size  $n$ , generated as a function of time by labile bridge scission, is calculated from the bridge population parameters  $\xi$  and  $p$  as follows:

$$m_{frag,n} = n m_a + (n - 1) m_b \left( \frac{\xi}{p} \right) + \frac{m_b}{4 (1 - p)} \quad (32)$$

The terms are defined in the nomenclature. The first term in Eq. 32 represents the molecular weight of the  $n$  clusters in a fragment ( $n = 1$  is a monomer, such as benzene, toluene or naphthalene;  $n = 2$  is a dimer, such as two benzenes connected by an aliphatic bridge; etc.). The second term is the molecular weight of labile bridges  $m_b$  multiplied by the fraction of intact labile bridges  $(n-1)\xi/p$ . Finally, the third term provides the molecular weight of side chains to be released as gas, and is calculated from the fraction of side chains,  $r/2(1-p)$ , times the number of broken bridges, times the mass of each side chain  $m = m_b/2$ . The total mass associated with fragments of size  $n$  is the mass of the fragment  $m_{frag,n}$  multiplied by the population of those fragments, as follows:

$$m_{fin,n} = m_{frag,n} Q_n(p) = \left\{ n m_a + (n - 1) m_b \left( \frac{\xi}{p} \right) + \frac{m_b}{4 (1 - p)} \right\} Q_n(p) \quad (33)$$

In this equation,  $Q_n(p) = F_n(p)/n$  is the population of  $n$ -cluster fragments, expressed on a per cluster basis.<sup>9</sup> The total mass associated with the finite fragments (assumed to be the tar mass in earlier descriptions of the CPD model<sup>6,45</sup>) is obtained by summing the contributions from each fragment size, as follows:

$$m_{fin}(t) = \sum_{n=1} m_{fin,n}(t) \quad (34)$$

Using Eqs. 5,8 and 9 to evaluate the sums over  $n$  in Eq. 34, the total mass of finite fragments on a per site basis is:

$$m_{fin}(t) = m_a F(p) + m_b K(p) \quad (35)$$

where  $F(p)$  and  $K(p)$  are obtained by rearranging and collecting terms in Eq. 33 to obtain:

$$F(p) = 1 + r \left[ \frac{\xi}{p} + \frac{(n-1)}{4(1-p)} \right] \quad (36)$$

$$K(p) = \left[ \frac{r}{2(1-p)} - \frac{\xi}{p} \right] \quad (37)$$

and  $r = m_b / m_a$  is the ratio of bridge mass to site mass. The variables  $F(p)$  and  $K(p)$  are defined earlier in Eqs. 5 and 9.

The mass fraction of gas, finite fragments, and char may now be calculated from:

$$f_{gas}(t) = \frac{m_{gas}(t)}{m_{total}} = \frac{r g (c_0 + 1)}{4 + 2 r (1 - c_0) (c_0 + 1)} \quad (38)$$

$$f_{fin}(t) = m_{fin}(t) / m_{tot}(t) = \frac{2}{2 + r(1 - c_0)(\epsilon + 1)} [F(p) + K(p)] \quad (39)$$

with

$$f_{char}(t) = [1 - f_{gas}(t) - f_{fin}(t)]. \quad (40)$$

The explicit dependence upon  $m_a$  and  $m_b$  is eliminated in the fractional weight quantities [i.e.  $f_{gas}(t)$ ,  $f_{tar}(t)$  and  $f_{char}(t)$ ] by dividing through with  $m_{total}$ . The designation of char used here applies to the portion of the coal contained in infinite arrays after the finite molecular clusters have been identified and contains both charred and unreacted labile bridges.

The ultimate yield of light gas is given by  $g(\infty) = 2(1 - c_0)$ , since both  $\epsilon(\infty)$  and  $\epsilon(\infty)$  would be zero at infinite time. The estimate of the ultimate light gas yield provides input to the analysis which allows  $r$  to be calculated for the values  $\epsilon$  and  $c_0$  using Eq. 38 to obtain the relationship:

$$r = 2f_{gas}(\infty) / \left\{ (1 - c_0)(\epsilon + 1) [1 - f_{gas}(\infty)] \right\} \quad (41)$$

and using Eqs. 38 and 39 with the condition that  $\epsilon = 0$  and  $\epsilon = 1$  for  $t = \infty$ , the ultimate yield of finite fragments is

$$f_{tar}(\infty) = [1 - f_{gas}(\infty)] F(p) \Big|_{t=\infty} \quad (42)$$

where the finite fragment population is given by the  $F(p)$  term obtained from percolation theory with  $p = c(\infty)$ .

### III. Tar Release

**a. Background.** The material extracted from parent coals using suitable solvents (such as tetrahydrofuran) corresponds to the bitumen, or finite fragments trapped in the coal at room temperature and pressure. This material is the first to vaporize from the coal as it is heated, since no bonds are broken to form the finite fragments prior to vaporization.<sup>49</sup> Many highly polar solvents such as pyridine extract colloidal dispersions along with the bitumen, which are agglomerates of material with extremely large molecular weights ( $\sim 10^6$  amu), and hence extract yields using such solvents are not representative of material that would vaporize during heating. Hence, in the CPD model, unlike in other models,<sup>16,18</sup> pyridine extract yield data are not used as input parameters. The initial mass fraction of finite fragments in the parent coal is calculated in the CPD model from the bridge population parameters  $\epsilon_0$ ,  $c_0$ , and  $f_{gas}$ , using percolation statistics.

The finite fragments formed as a result of bridge scission may undergo a phase change to form a vapor, dependent upon the pressure, temperature, and molecular weight. At a given temperature and pressure, the low molecular weight species (e.g., benzene, naphthalene) have high vapor pressures, causing significant quantities to be released as vapor. As pyrolysis products are cooled to room temperature and pressure, however, many of these species condense to form liquids and solids, and hence are classified as tar. Species that do not condense at room temperature and

pressure are considered light gas, and are treated separately.<sup>6</sup> High molecular weight species with low vapor pressures that do not vaporize at reaction temperatures and pressures remain in a liquid or solid state in the char matrix. Hence, a fragment of intermediate molecular weight may be metaplast at one temperature and tar vapor at an elevated temperature. The non-vaporized material that is detached from the infinite coal matrix is termed metaplast.

In the present work, the effect of vapor pressures on gas phase pyrolysis products is modeled assuming a simple form of Raoult's law, requiring the development of an empirical expression describing the vapor pressures of high molecular weight organic molecules (in the range 200 to 1000 amu). Previous generalized vapor pressure expressions were developed for only a limited set of species at very low pressures. The Raoult's law expression and the vapor pressure correlation are combined with a standard flash distillation calculation at each time step to determine the partitioning between vapor and liquid for each finite fragment size. Equilibrium between escaped tar and trapped metaplast is used to demonstrate the capability of this improved CPD model to describe pressure-dependent tar yields and molecular weight distributions. The Raoult's law formulation, development of the generalized vapor pressure expression, and the flash distillation equations are described below.

**b. Raoult's Law.** In a treatment similar to the flash vaporization scheme proposed by Niksa,<sup>15</sup> it is assumed that the finite fragments undergo vapor/liquid phase equilibration on a time scale that is rapid with respect to the chemical bond scission reactions. As an estimate of the amount of vapor and liquid present at any time, Raoult's law is invoked; the partial pressure  $P_i$  of a substance is proportional to the vapor pressure of the pure substance  $P_i^v$  multiplied by the mole fraction of the substance in the liquid  $x_i$ :

$$P_i = y_i P = x_i P_i^v \quad (43)$$

where  $y_i$  is the mole fraction of the species in the vapor phase. This simple form of Raoult's law neglects activity coefficients, since this type of data is not generally available for large molecular weight organic species. The total pressure  $P$  is the sum of the partial pressures of the different gaseous species:

$$P = \sum_{i=1} y_i P = \sum_{i=1} P_i \quad (44)$$

**c. Vapor Pressures of High Molecular Weight Organic Molecules.** Vapor pressure data for coal tar are unavailable, so vapor pressure correlations based on compounds found in coal tar are generally used. Unger and Suuberg<sup>50</sup> proposed a vapor pressure correlation based on boiling points of six aromatic hydrocarbons<sup>51</sup> at a total pressure of  $6.6 \times 10^{-4}$  atm (0.5 mm Hg). These compounds were selected because of their high molecular weight (198 to 342) and their lack of heteroatoms. The resulting correlation developed by Unger and Suuberg is:

$$P_i^y = \exp\left(-\frac{M_i^y}{T}\right) \quad (45)$$

where  $\Delta H_i^y = 5756$ ,  $\Delta S_i^y = 255$ , and  $\Delta G_i^y = 0.586$ , and units are in atmospheres and Kelvin. The form of Eq. 45 can be obtained from the Clausius-Clapeyron equation, assuming that the heat of vaporization is proportional to molecular weight. Equation 45 is the simplest thermodynamic expression relating vapor pressure, temperature, and molecular weight,<sup>52</sup> and is used because of the lack of detailed chemical structure and vapor pressure data on coal tar.

Several investigators have attempted to use the Unger-Suuberg correlation to describe tar release from metaplast. Many investigators use the form of the Unger-Suuberg correlation, but not the constants proposed by Unger and Suuberg. Solomon and coworkers<sup>18</sup> used the Unger-Suuberg correlation multiplied by a factor of 10 in order to fit tar and total coal volatiles yields as a function of pressure, although recently the factor of 10 was eliminated by changing other input parameters.<sup>53</sup> Niksa<sup>15</sup> used a similar form that was easy to integrate analytically, with  $\Delta H_i^y = 1$ , and  $\Delta S_i^y$  and  $\Delta G_i^y$  as adjustable parameters to fit tar molecular weight data from Unger and Suuberg.<sup>54</sup> All three vapor pressure coefficients are treated as adjustable parameters in recent work by Niksa.<sup>16</sup> Oh and coworkers<sup>55</sup> and Hsu<sup>56</sup> found that by using the Unger-Suuberg correlation, good agreement could be achieved with high temperature pyrolysis data ( $T > 873$  K) but not with low temperature data ( $T < 873$  K). The current work suggests why the validity of the Unger-Suuberg correlation is limited, and gives a similar but alternate correlation.

The vapor pressure correlation of Unger and Suuberg<sup>50</sup> is based on data at low vapor pressures (0.5 mm Hg), but has been extrapolated to much higher pressures and molecular weights in coal devolatilization models. Reid, et al.<sup>52</sup> recommend using the Antoine equation to calculate vapor pressures (if constants are available) when the vapor pressure is in the range 10 to 1500 mm Hg (.01 to 2 atm). However, Reid and coworkers conclude that no correlation produces good agreement with data for  $P_i^y < 10$  mm Hg (.01 atm). The approach used here is to develop new constants for Eq. 45 based on additional data at both low and high vapor pressures in order to treat to a wide range of coal pyrolysis conditions. The use of the resulting vapor pressure correlation eliminates some of the uncertainties in developing input parameters for coal pyrolysis models.

Gray, et al.<sup>57,58</sup> measured vapor pressures as a function of temperature for twelve narrow boiling fractions distilled from coal liquids produced from SRC-II processing of Pittsburgh seam bituminous coal. In their study, temperatures ranged from 267 K to 788 K, the coal liquids exhibited molecular weights ranging from 110 to 315 amu, and the lightest fractions exhibited vapor pressures as high as 35 atm. It is assumed that these are representative of low molecular weight tars released during primary pyrolysis. Gray and coworkers discuss equations of state that fit the vapor pressure data using critical properties of the liquid (i.e., the critical temperature and pressure). However, for the purposes of coal pyrolysis, critical properties are not well known, and simpler correlations are needed.

A new correlation was generated by curve-fitting the data of Gray, et al.<sup>57,58</sup> using Eq. 45; the new coefficients are shown in Table 1. This correlation, referred to as the Fletcher-Grant-Pugmire

(FGP) correlation, agrees well with the measured vapor pressures of the different molecular weight fractions, as shown in Fig. 7. Coefficients for the vapor pressure expressions used by other investigators are also shown in Table 1. It is interesting that the coefficient on the molecular weight ( ) from the curve-fit to the data of Gray and coworkers is 0.590, which is very close to the value of 0.586 found by Unger and Suuberg. The value of from the Unger-Suuberg correlation is 255, which compares reasonably well with the value of 299 in FGP correlation. The major difference between the two correlations is the value for FGP is fifteen times greater than that found in the Unger-Suuberg correlation. This is somewhat consistent with modeling efforts<sup>11</sup> where the vapor pressure from Unger-Suuberg correlation was multiplied by a factor of 10 in order to achieve agreement with a wide range of experimental data.

**Table 1**  
**Vapor Pressure Correlations for Coal Pyrolysis Tar and Metaplast**

$P_i^v = \exp\left(\frac{-MW_i}{T}\right)$			
	(atm)	(g <sup>-</sup> mole K)	
Unger-Suuberg <sup>16</sup>	5756	255	0.586
Niksa <sup>15</sup>	70.1	1.6	1.0
Niksa and Kerstein <sup>16</sup>	$3.0 \times 10^5$	200	0.6
FGP (this work)	87,060	299	0.590

The FGP vapor pressure correlation was also compared with boiling point data at pressures of 5, 60, 760, and 7600 mm Hg (0.0066, 0.079, 1.0, and 10 atm) for a set of 111 pure organic compounds of the type that are thought to be present in coal-derived liquids. Boiling point data are from Perry and Chilton;<sup>59</sup> a list of the selected compounds is available.<sup>60</sup> Molecular weights as high as 244 are considered in this set of compounds. Long chain alkanes (hydrogen to carbon ratios greater than 1.5) and heteroatoms with more than two oxygen atoms are not considered in this data set, since they are not believed to occur in coal tars to a significant extent. Boiling point data at 10 atmospheres are only available for five compounds.<sup>25</sup> The FGP correlation was found to agree surprisingly well with the boiling points of these compounds at all four pressures, as shown in Fig 8. This is a simplistic vapor pressure expression; other vapor pressure expressions that take into account the variations in the chemical structures of the various compounds<sup>52</sup> are not considered. The correlation proposed by Unger and Suuberg<sup>50</sup> agrees with this set of data at the lowest pressure, but predicts higher boiling points than the data at pressures of 1 and 10 atm (see Fig. 8).

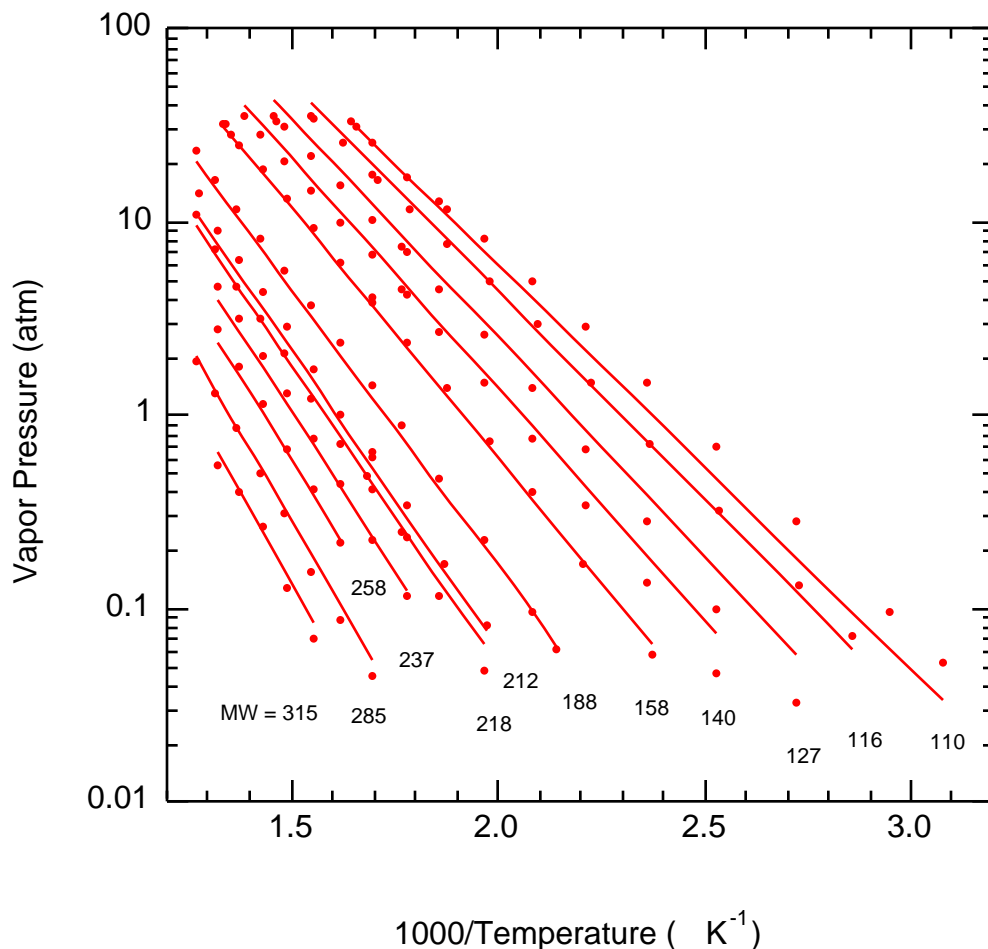


Figure 7. Comparison of the Fletcher-Grant-Pugmire vapor pressure correlation with vapor pressure data from Gray, et al.<sup>57,58</sup> for twelve narrow boiling fractions of coal liquids from a Pittsburgh seam coal.

The six data points used to develop the Unger-Suuberg correlation<sup>50</sup> were taken from Smith, et al.,<sup>51</sup> the FGP correlation also agrees well with these same six data points. The sum-square error of the FGP correlation with regard to these six boiling points is actually 12% less than that obtained using the Unger-Suuberg correlation. The similarity of the two correlations at low vapor pressures suggests the need for careful examination of the two correlations versus data at a wide range of temperatures and pressures. The Unger-Suuberg correlation was found to yield poor agreement with the data of Gray, et al.<sup>57,58</sup> where the predicted vapor pressures were three times lower than the data at 35 atm.

Coal pyrolysis experiments have been conducted at pressures as high as 69 atm,<sup>61</sup> with reported tar molecular weight distributions extending into several thousand amu. Figure 9 shows an extrapolation of three vapor correlations to higher temperatures, pressures, and molecular weights than shown in Fig. 8, representing a wide range of pyrolysis conditions. The difference between

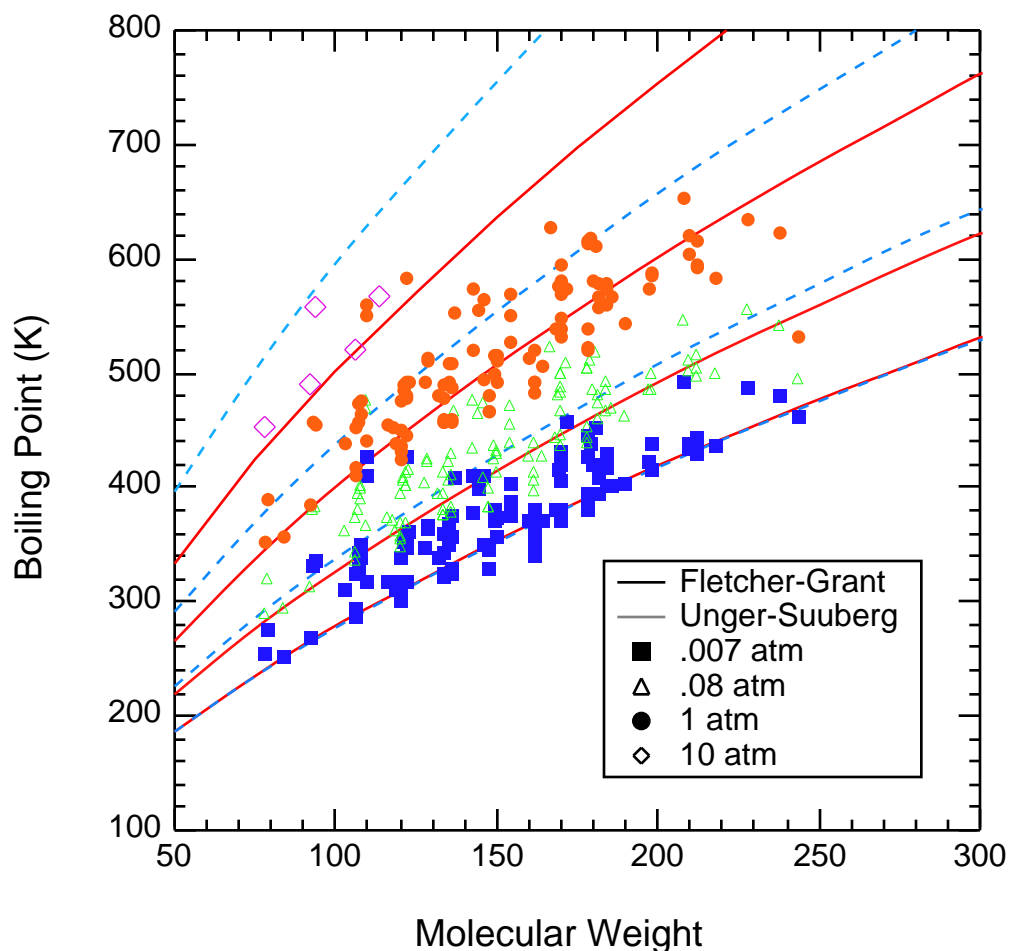


Figure 8. Comparison of the Fletcher-Grant-Pugmire vapor pressure correlation and the Unger-Suuberg vapor correlation with boiling point data for 111 organic compounds at pressures of .007, .08, 1, and 10 atm (5, 60, 760, and 7600 mm Hg).

the FGP correlation and the Unger-Suuberg correlation becomes more pronounced at higher pressures. For example, the predicted boiling point of a species with a molecular weight of 400 amu by the FGP correlation is nearly 500 K lower than that predicted by the Unger-Suuberg correlation. In contrast, the parameters in the vapor pressure correlations used by Niksa<sup>15,16</sup> were used as fitting parameters to achieve agreement with measured molecular weight distributions. In FLASCHCHAIN, two sets of vapor pressure coefficients are presented: one set for predictions with recombination kinetics, and one set when recombination kinetics are neglected. The boiling points predicted by the correlations used by Niksa and Kerstein<sup>16</sup> at a pressure of one atmosphere closely follow the 0.007 atm curve from the FGP correlation in Fig. 9, and are not shown. For a molecular weight of 400 amu, the two Niksa correlations<sup>15,16</sup> give boiling points at atmospheric pressure that are respectively 800 K and 300 K lower than predicted by the FGP correlation, illustrating that unrealistic solutions can be obtained when vapor pressure coefficients are used as

adjustable parameters. The FGP vapor correlation agrees with measured vapor pressures of coal liquids and boiling points of pure compounds over a wide range of pressures. The coefficients  $\alpha$ ,  $\beta$ , and  $\gamma$  used in the correlation are fixed by independent data, thereby reducing the number of unknown parameters in coal pyrolysis models.

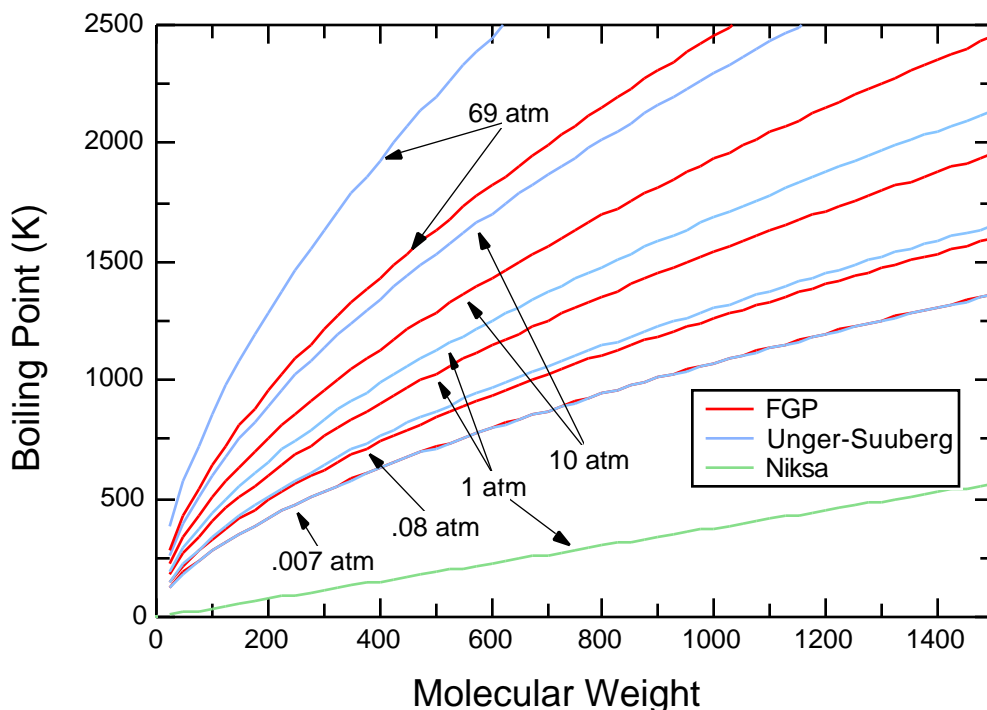


Figure 9. Comparison of the FGP (this work), Unger-Suuberg,<sup>50</sup> and Niksa<sup>15</sup> vapor correlations for molecular weights as high as 1500 and pressures as high as 69 atm.

**d. Flash Distillation.** The mass of finite fragments can be used as the feed stream of a flash distillation process, where vapor-liquid equilibrium is achieved. The approach to flash distillation is patterned after the method outlined by King.<sup>62</sup> If  $f_i$  = the moles of species  $i$  before vapor-liquid equilibrium,  $l_i$  = the moles of species  $i$  in the metaplast after vapor-liquid equilibrium, and  $v_i$  = the moles of species  $i$  in the vapor phase after vapor-liquid equilibrium, then the following relations apply:

$$f_i = v_i + l_i \quad (46)$$

$$F = V + L \quad (47)$$

where

$$F = \sum_i f_i, \quad V = \sum_i v_i, \quad L = \sum_i l_i \quad (48)$$

and

$$f_i = z_i F, \quad v_i = y_i V, \quad l_i = x_i L \quad (49)$$

Vapor-liquid relationships are expressed in the form:

$$y_i = K_i x_i \quad (50)$$

In this treatment, Raoult's law (Eq. 43) is used to calculate values of  $K_i$  as a function of time, based on the current particle temperature and ambient pressure. Substituting the expression for  $y_i$  (Eq. 50) into Eq. 46 yields

$$z_i F = K_i x_i V + x_i L = x_i (F - V) + x_i K_i V \quad (51)$$

This equation is rearranged to provide an expression for  $x_i$ :

$$x_i = \frac{z_i}{(K_i - 1) \frac{V}{F} + 1} \quad (52)$$

Following recommendations by Rachford and Rice,<sup>63</sup> the identity

$$\sum_i y_i - \sum_i x_i = 0 \quad (53)$$

can be used with Eqs. 50 and 52 to provide a stable equation for iterative numerical solution:

$$f\left(\frac{V}{F}\right) = \sum_i \frac{z_i (K_i - 1)}{(K_i - 1) \left(\frac{V}{F}\right) + 1} \quad (54)$$

This equation is in a form with relatively linear convergence properties, with no spurious or imaginary roots.<sup>62</sup> Other forms of solution present highly nonlinear functions, which often lead to imaginary roots. The secant method (e.g., Gerald<sup>64</sup>) is used to solve for  $V/F$  from Eq. 54, and Eqs. 50 and 52 are used to obtain  $x_i$  and  $y_i$ .

**e. Mass Transport Considerations.** The application of the flash distillation equations to coal tar evolution requires appropriate assumptions regarding the location and amount of material that is in vapor-liquid equilibrium. Different theoretical treatments of mass transfer effects on coal tar evolution are reviewed by Suuberg.<sup>4</sup> For example, Oh, et al.<sup>55</sup> and Hsu<sup>56</sup> used bubble transport models to describe intraparticle transport of tar and gases. In a different approach used by Solomon, et al.<sup>18</sup> and by Niksa,<sup>15,16</sup> the tar vapor is convected only by the light gas, and it is assumed that the volume of vaporized tar is insignificant compared to the volume of evolved light gas. If tar vapor is formed, but no light gases are formed at the same time, that approach implies that the tar vapor is trapped within the particle. Other approaches allow for the possibility that some liquid from the metaplast may be entrained in the light gas in an attempt to explain reported molecular weights greater than 1000 amu,<sup>4</sup> where the molecular weight is too high to allow vaporization.

In the CPD model, the assumption is made that all gaseous species (light gases and tar vapors) are convected away from the particle due to the increase in volume between the gas and solid. The convection step is assumed to be rapid compared with the chemical reactions of bond scission and char formation. Convection of liquid metaplast by gases and tar vapors is thought to be of secondary importance, based on recent measurements of tar molecular weights,<sup>18,21</sup> and is ignored in this work. This is consistent with experimental results of Suuberg, et al.,<sup>65</sup> which indicate that tar evaporation is more important than transport of liquid tar by light gas. The vapor pressures predicted by the FGP correlation drop steeply with molecular weight, implying that there is little vaporization of high molecular weight compounds. In other words, most of the tar vapor at a given temperature consists of compounds with vapor pressures higher than the ambient pressure. It is assumed that the volume of tar vapor alone is sufficient to cause rapid evolution from the vicinity of the particle, without the necessity of transport by lighter gases. The presence of light gas is not necessary for tar release by a convective flow mechanism, since the phase change from liquid metaplast to tar vapor increases the volume by two to three orders of magnitude.

Only the tar and light gas formed in the last time step are considered to be in vapor-liquid equilibrium with the metaplast. This is analogous to a plug flow reactor, in that the tar and light gas formed at earlier residence times does not mix with newly-formed pyrolysis products. The amount and molecular weight distribution of the tar and light gas formed at each time step is stored for use in the flash distillation calculation of the next time step. The computed results are therefore time-step dependent unless care is taken to use small time increments during periods of rapid tar release. In order to maintain computational efficiency, a numerical scheme was implemented that adjusts the time step based on the rate of reaction.

**f. Crosslinking.** Large amounts of high molecular weight compounds are generated during the pyrolysis of bituminous coals, as evidenced by solvent extraction experiments. Fong and coworkers<sup>67</sup> measured the amount of pyridine extracts from coal chars as a function of residence time at moderate heating conditions (~ 500 K/s). A maximum of 80% of the original coal was either released as volatile matter or extracted with pyridine during these experiments. However, at the completion of volatiles release, very small amounts of pyridine extractables were obtained. The final volatiles yield was approximately 40% in these experiments; the additional amount of pyridine extractables (approximately 40%) was in some manner crosslinked to the char matrix before the end of devolatilization. The pyridine extract data are viewed as a qualitative description of the

amount of metaplast existing in the coal. However, pyridine extracts contain significant quantities of colloidally dispersed material (molecular weights of  $10^6$  amu or higher), and hence these data should not be used quantitatively.

Additional experiments have been performed to characterize the extent of crosslinking in coal chars during devolatilization. Solvent swelling measurements of coal chars are interpreted as indications of the extent of crosslinking.<sup>67</sup> Solid state  $^{13}\text{C}$  NMR measurements of the chemical structure of coal chars also show an increase in the number of bridges and loops between aromatic clusters in the final stages of mass release,<sup>29,31</sup> indicative of crosslinking. The importance of crosslinking was illustrated in a recent comparison of earlier formulations of the CPD model that did not treat crosslinking with models that include treatments of crosslinking.<sup>68</sup>

A simple crosslinking model is used in this work to account for the reattachment of metaplast to the infinite char matrix. The rate of crosslinking is represented by a simple, one-step Arrhenius rate expression:

$$\frac{dm_{\text{cross}}}{dt} = - \frac{dm_{\text{meta}}}{dt} = k_{\text{cross}} m_{\text{meta}} \quad (55)$$

where  $m_{\text{meta}}$  is the mass of metaplast,  $m_{\text{cross}}$  is the amount of metaplast that has been reattached to the infinite char matrix, and  $k_{\text{cross}}$  is the Arrhenius rate constant [ $k_{\text{cross}} = A_{\text{cross}} \exp(-E_{\text{cross}}/RT)$ ].

The mass of metaplast is updated at each time step, based on: (1) the amount of finite fragment material generated during labile bridge scission, according to the percolation statistics, and (2) the flash distillation submodel and vapor pressure relationship. The amount of metaplast that has been reattached to the infinite char matrix during each time step is calculated and added to the mass of the char. For simplicity, the metaplast that is reattached to the char is assumed to uniformly decrease the concentration of all fragment size bins on a mass basis. In other words, one rate of reattachment (on a mass basis) is used, independent of fragment size. In reality, the fragments containing many clusters contain the most sites for reattachment,<sup>6</sup> and should therefore crosslink faster (on a number basis) than compounds with one or two clusters. However, since the concentration of each fragment size decreases monotonically with the number of clusters, very few fragments with large numbers of clusters exist. At the present time, there is no mechanistic or empirical basis for the use of separate crosslinking rates for each fragment size bin, and errors introduced by assuming uniform crosslinking rates are thought to be small.

The crosslinking mechanism in the CPD model is decoupled from the percolation statistics. For bituminous coals, the crosslinking occurs subsequent to tar release,<sup>29,31</sup> meaning that the labile bridge scission and the reattachment of finite clusters occur in series. For low rank coals, such as lignites, there is evidence for crosslinking before significant tar release.<sup>31,67,69</sup> This type of early crosslinking is treated in the selection of initial chemical structure parameters for the CPD model, and will be treated formally in a subsequent investigation.

It is assumed that the crosslinking process does not introduce an additional mechanism for light gas release, so that the population of side chains is not affected by the crosslinking reaction. However,

tar that is released from the particle may contain labile bridges ( $\ell$ ), char bridges ( $c$ ), and side chains ( $s$ ). The initial description of the CPD model allowed for reactions of tar in the gas phase after release from the particle.<sup>6,45</sup> In this work, secondary tar reactions in the gas phase are not treated in order to permit comparison with devolatilization experiments such as heated grids where the tar is quenched after leaving the vicinity of the particle. The side chains released with the tar must therefore be subtracted from the pool of side chains available to form light gas from the char and metaplast. The number of side chains,  $s$ , is calculated from the percolation statistics, which are decoupled from the flash distillation and crosslinking mechanisms, as described earlier in Eq. 15:

$$\frac{d}{dt} = \frac{2}{(s + 1)} k_b \ell - k_g \quad (56)$$

where  $k_g$  is the rate constant for light gas formation from side chains ( $g_1$ ), and other terms are described in the nomenclature. The first term on the RHS of Eq. 56 represents the formation of side chains due to labile bridge scission, and the second term represents the release of side chains as light gas,  $g_1$ . The mass of light gas formed from side chains is calculated from an algebraic relationship (same as Eq. 21):

$$g_1 = 2(1-p) - \quad (57)$$

where  $p$  is the number of intact bridges ( $\ell + c$ ). The first term in Eq. 57 represents the total number of broken labile bridges (which are split into two pieces) and the second term represents the number of side chains remaining. Additional light gas,  $g_2$ , is released during the stabilization of labile bridges to form char bridges. The amount of light gas formed during char formation is calculated from the change in the char bridge population as given in earlier Eq. 22.

In the initial description of the CPD model,<sup>6,45</sup> the labile bridges and side chains in the evolved tar continued to react at the same temperature as the particle; a gradual decrease in tar yield was accompanied by a corresponding increase in gas yield at long residence times. In a combustion environment, this simulates the thermal cracking of tar and the initial stages of soot formation. However, in the present formulation, gas phase reaction of tar is not calculated, and only the amount of gas released from the char and metaplast is treated. In order to account for the decrease of gas precursors as tar is released, the mass of gas formed ( $m_{gas}$ ) is normalized by the tar yield as follows:

$$m'_{gas} = m_{gas}(1 - f_{tar}) \quad (58)$$

where  $f_{tar}$  is the mass fraction of coal evolved as tar and  $m'_{gas}$  is the normalized amount of gas. This is an approximate normalization procedure, and assumes that the concentrations of labile bridges, char bridges, and side chains in the tar are equal to the respective concentrations in the combination of metaplast, crosslinked metaplast, and the infinite char lattice. This assumption is good to first order, but small errors are introduced because the tar consists of only the light molecular weight fragments (monomers and dimers), and hence should contain a slightly different

concentration of side chains than the metaplast and infinite char lattice. The alternative to this assumption is an extensive accounting procedure of molecular fragment bins with appropriate exchange coefficients, as used by Niksa and Kerstein.<sup>16</sup> Errors introduced by this assumption are small and the CPD model does not contain this complexity for the present.

**g. Computational Details.** The time-dependent differential equations for  $\xi$ ,  $c$  and  $\dots$  (Eqs. 11, 14, and 15) are solved numerically using the modified Euler predictor-corrector method.<sup>64</sup> The other dynamic variables ( $p$ ,  $g_1$ ,  $g_2$ ) may be obtained from the first three variables using algebraic expressions (Eqs. 18-22). The required computational time on a VAX 11/780 is short (less than 5 sec of CPU time) for a typical simulation. The input data include gas, tar and char yields along with particle temperatures as a function of residence time.

The activation energies used in this model are distributed to correspond with the changing distribution of bond strengths as the species evolve. The chemical reactions with distributed energies are viewed as progressing sequentially, with the low-activation-energy species reacting at lower temperatures, followed by the high-activation-energy species. Thus, the specific activation energy of these reactions is increased according to a normal distribution function as the reactions proceed. The normalized probability function, therefore, is given as follows:

$$\frac{d_i}{d_{i \max}} = \frac{1}{\sqrt{2} V_i} \int_0^E \exp \left\{ -\frac{1}{2} \left( \frac{E - E_i}{V_i} \right)^2 \right\} dE \quad (59)$$

where  $E_i$  and  $V_i^2$  are the mean activation energy and its variance, respectively, for the  $i$ th distributed process to be determined for  $d_i/d_{i \max}$ , the ratio of any distributed variable to its maximum value. Equation 59 represents the fractional area under a normal curve for the appropriate value of  $E$ , and is coded in the form of a look-up table using the transformation

$$z = \frac{E - E_i}{V_i} \quad (60)$$

For any extent of reaction indicated by  $d_i/d_{i \max}$ , the activation energy is calculated from tabulated values of the area under the normal curve represented in Eq. 59. For example, the activation energy is set equal to  $E_i$  when 50% of the reaction is completed. This method used for distributing activation energies allows the rates to change as the reaction proceeds without the necessity of solving a complex distribution function involved in traditional DAEM methods.\*\* Using the above distribution for the gas release activation energy,  $d_i/d_{i \max}$  for the gas release is given by

$$g/g_{\max} = g/g(\ ) = g/2(1 - c_0) \quad (61)$$

The corresponding  $d_i/d_{i \max}$  for the bridge-breaking reaction becomes  $(1 - \xi/\xi_0)$ .

---

\*\* The authors used this assumption to simplify the computational details. This approach is somewhat unconventional; the effect on the model of the traditional integral form of the distributed activation energy needs to be explored.

## IV. Selection of Model Input Parameters

The relation of model input parameters to actual chemical and physical properties of the coal, developed below, establishes the mechanistic basis of the model and facilitates extrapolation to other coal types and operating conditions.

**a. Kinetic Rate Parameters.** Use of the CPD model requires specification of three rates: the rate of labile bridge scission, the rate of light gas release, and the rate of crosslinking. These kinetic rates are assumed to be coal-independent; only the chemical structure determines differences in devolatilization behavior due to coal type. In addition, the composite rate coefficient relating the rate of side chain formation to the rate of char bridge formation must also be specified. A discussion of the rate parameters for the bridge scission, gas release, and char formation reactions is provided in earlier publications.<sup>6,45</sup> The value of  $E_b$  in the CPD model was set at 55 kcal/mole, as reported by Serio. A weighted-average of the activation energies for light gas release reported by Serio resulted in  $E_g = 69$  kcal/mole. The data of Serio et al.<sup>5</sup> were curve-fit using the CPD model to obtain values for  $A_b$ ,  $V_b$ ,  $A_g$ , and  $V_g$ . Results of this evaluation are shown in Figs. 10-12, with resulting kinetic parameters given in Table 2. As shown by Fletcher, et al.,<sup>45</sup> these kinetic parameters allow good agreement between predicted and measured coal devolatilization rates for heating rates ranging from 1 K/s to  $10^4$  K/s. For example, a comparison of CPD model predictions with the data of Fletcher,<sup>70,71</sup> which include measurements of single particle temperatures, is shown in Fig. 13 for Illinois #6 coal particles (106-125  $\mu\text{m}$  size fraction). As discussed below, chemical structure parameters for these model predictions were taken directly from NMR data, which was not possible with earlier model formulations that did not treat vapor-liquid equilibrium and crosslinking.

**b. Crosslinking Rates.** The use of the crosslinking mechanism in the CPD model requires specification of two additional rate parameters:  $E_{cross}$  and  $A_{cross}$ . Solomon and coworkers<sup>18</sup> used solvent swelling data to generate an empirical correlation between the rate of  $\text{CH}_4$  release and the rate of crosslinking in high rank coals ( $E_{\text{CH}_4} = 60$  kcal/mol). Other investigators have taken crosslinking rates from time-dependent pyridine extractables from coal chars during devolatilization (Fong, et al.,<sup>66</sup>  $E_{cross} = 42$  kcal/mol) or from tar and total volatiles yields (Niksa and Kerstein;<sup>16</sup>  $E_{cross} = 50$  kcal/mol). This section describes the rationale for the selection of the values of  $E_{cross}$  and  $A_{cross}$  used in the CPD model, and illustrates the sensitivity of the model to these parameters.

The crosslinking in bituminous coals occurs subsequent to tar release, as evidenced by the NMR data regarding the number of bridges and loops per aromatic cluster as a function of mass release.<sup>29</sup> Therefore, the activation energy used for the crosslinking rate in the CPD model must be higher than that used for labile bridge scission (55 kcal/mol). A series of calculations was performed to determine the performance of the CPD model with three different values of  $E_{cross}$  (60, 65, and 70 kcal/mol). The pre-exponential factor  $A_{cross}$  was set to that used for gas release in the CPD model ( $3.0 \times 10^{15} \text{ s}^{-1}$ ); this high value assures rapid crosslinking after a threshold temperature is achieved. Model predictions using the three values of  $E_{cross}$  were compared with: (a) temperature-dependent total volatiles yield data at different heating rates;<sup>70</sup> (b) time-dependent, pyridine extract yield data;<sup>66</sup> and (c) NMR data regarding the number of bridges and loops per aromatic cluster.<sup>29</sup> Results and interpretations are as follows:

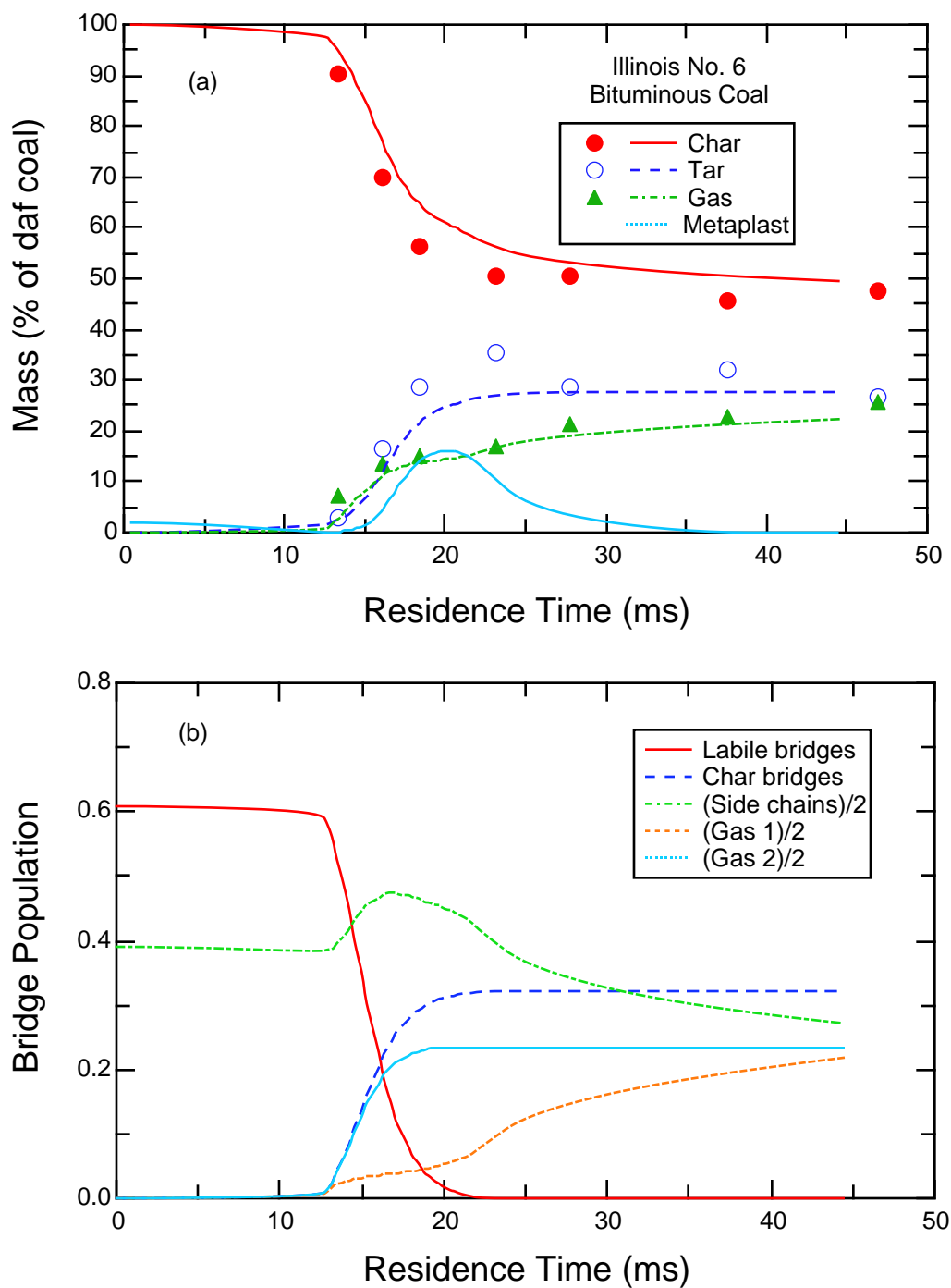


Figure 10. (a) CPD calculations of devolatilization yields of char, tar, and light gases versus time for Illinois No. 6 high-volatile bituminous coal. Experimental data are from Serio, et al.,<sup>5</sup> and chemical structure parameters for the model are taken directly from NMR data (no adjustable parameters); (b) Bridge dynamic population parameters on a per site basis as a function of time ( $\rho$ ,  $g_1$ , and  $g_2$  variables are divided by two).

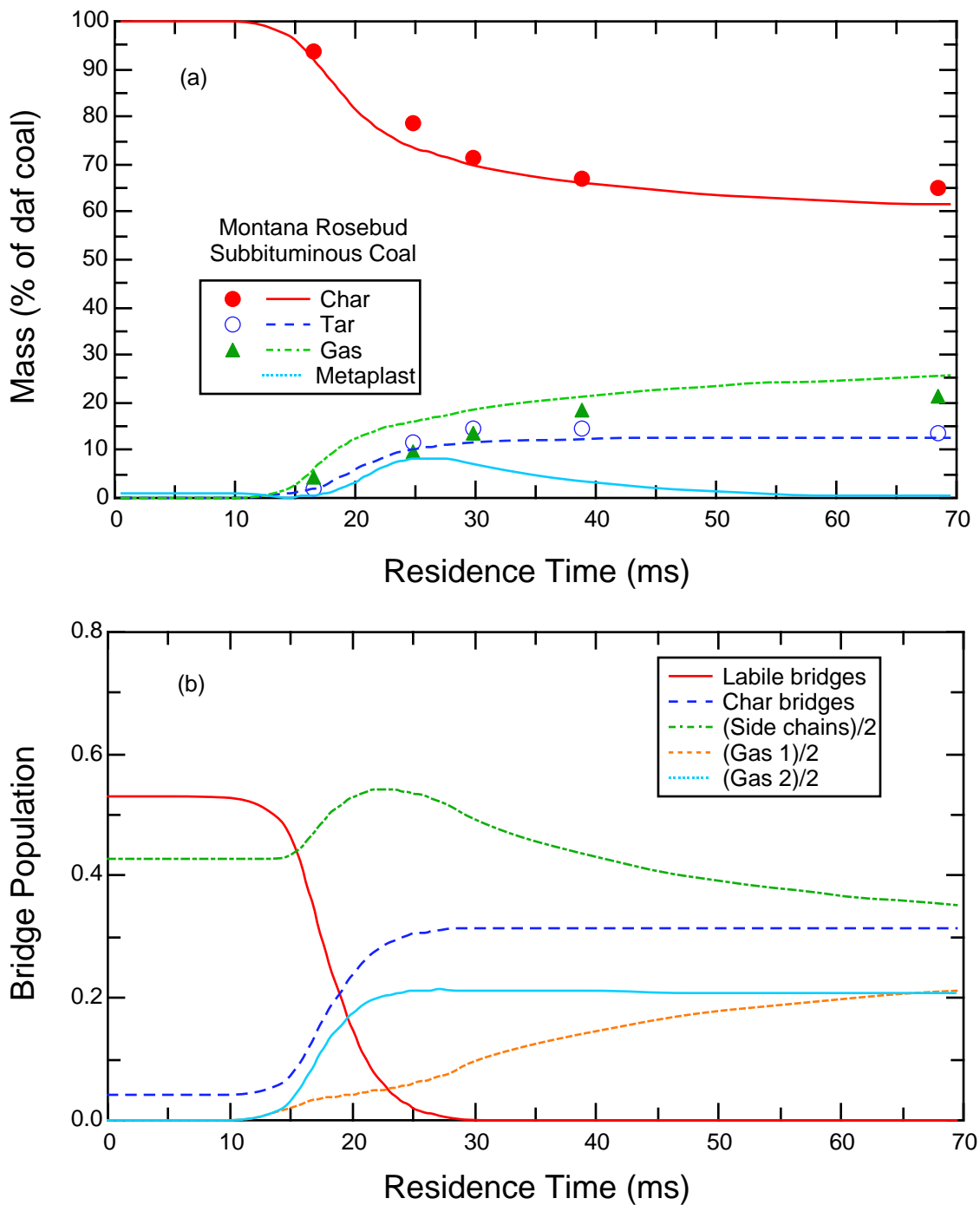


Figure 11. (a) CPD calculations of devolatilization yields of char, tar, and light gases versus time for Montana Rosebud subbituminous coal. Experimental data are from Serio, et al.,<sup>5</sup> and chemical structure parameters for the model are taken directly from NMR data (one adjustable parameter:  $c_0$ ); (b) Bridge dynamic population parameters on a per site basis as a function of time ( $c$ ,  $g_1$ , and  $g_2$  variables are divided by two).

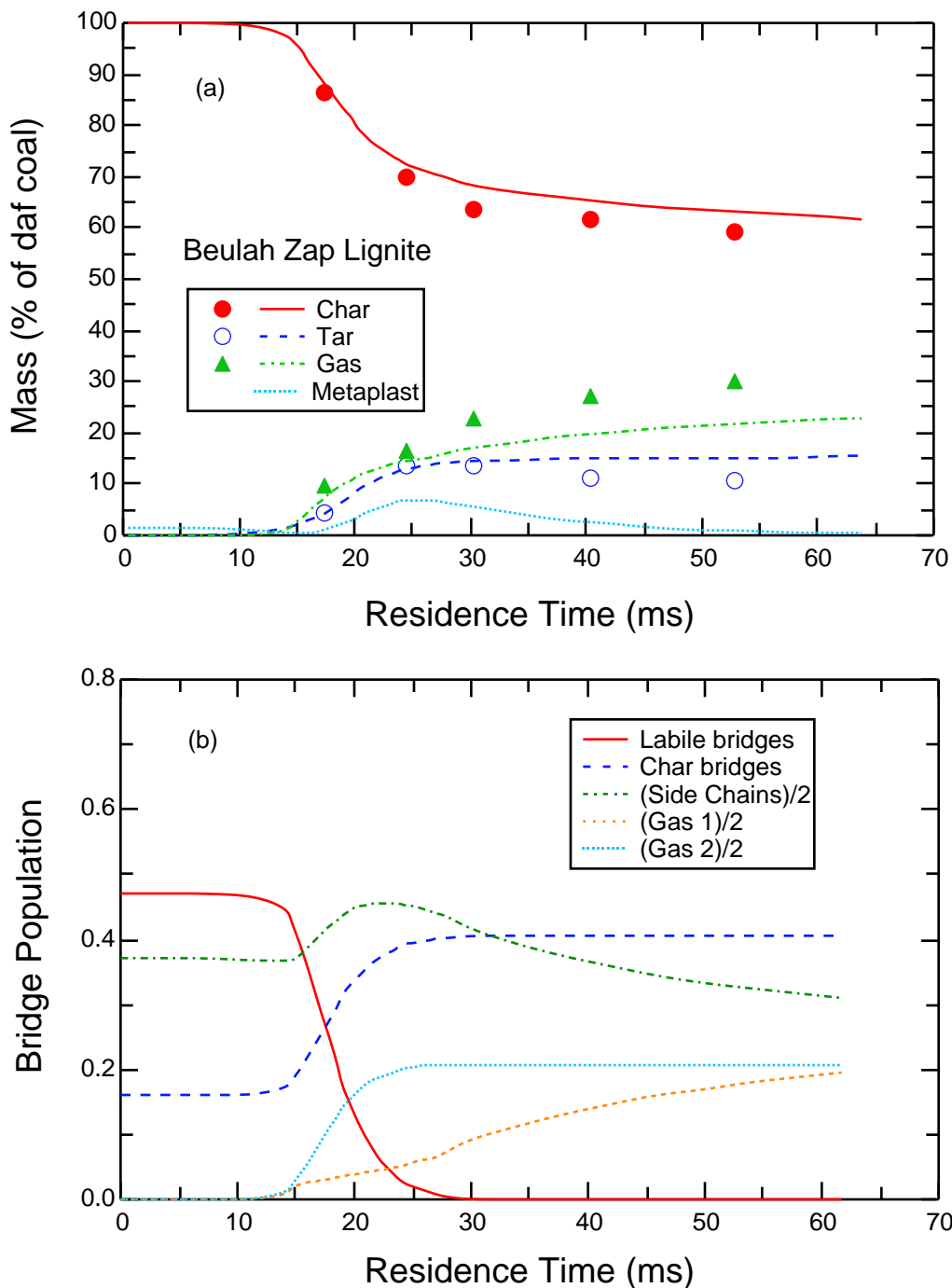


Figure 12. (a) CPD calculations of devolatilization yields of char, tar, and light gases versus time for North Dakota Beulah Zap lignite. Experimental data are from Serio, et al.,<sup>5</sup> and chemical structure parameters for the model are taken directly from NMR data (one adjustable parameter:  $c_0$ ); (b) Bridge dynamic population parameters on a per site basis as a function of time ( $g_1$  and  $g_2$  variables are divided by two).

**Table 2**  
**Rate Parameters Used in the CPD Model**

parameter	value	description
$E_b$	55.4 kcal/mol	Bridge scission activation energy
$A_b$	$2.6 \times 10^{15} \text{ s}^{-1}$	Bridge scission frequency factor
$b$	1.8 kcal/mol	Standard deviation for distributed $E_b$
$E_g$	69 kcal/mol	Gas release activation energy
$A_g$	$3 \times 10^{15} \text{ s}^{-1}$	Gas release frequency factor
$g$	8.1 kcal/mol	Standard deviation for distributed $E_g$
	0.9	Composite rate constant $k/k_c$

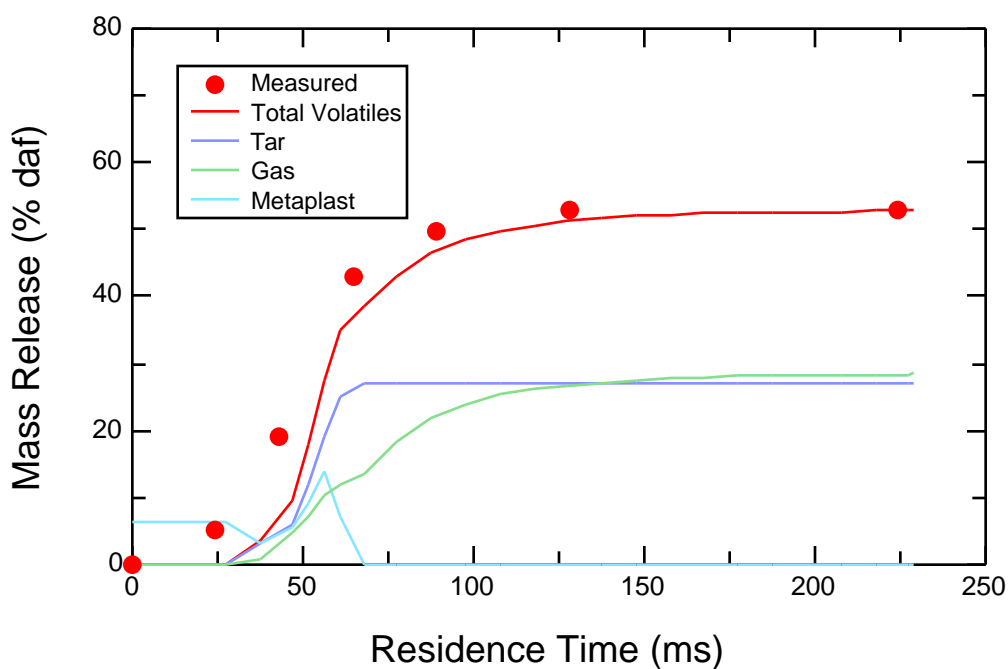


Figure 13. CPD model predictions (curves) of devolatilization yields of char, tar, and light gases versus time for Illinois #6 coal in the Sandia CDL. Experimental data (points) are from Fletcher;<sup>70,71,77</sup> and chemical structure parameters for the model are taken directly from NMR data (no adjustable parameters).

Volatiles Yield Data. Gibbins-Matham and Kandiyoti<sup>72</sup> measured total volatiles yields from a Pittsburgh No. 8 coal sample as a function of temperature for three conditions: (i) 1000 K/s with a 30 s hold time at the final temperature; (ii) 1000 K/s with a 0 s hold time (immediate quench); and (iii) 1 K/s with immediate quench. The coal used in these experiments was from the Argonne premium coal bank (-20 mesh), but was sieve classified to approximately 100  $\mu\text{m}$  in diameter. At temperatures lower than 800 K, the measured mass release at 1 K/s exhibits the same temperature dependence as the measured mass release at 1000 K/s with the 30 s hold. The initial mass release at 1000 K/s with no hold time at the peak temperature occurs at temperatures that are approximately 150 K higher than in the 30 s hold time experiment. The high temperature volatiles yield for the 1 K/s experiment was about 7% (daf) lower than in the 1000 K/s experiments.

An earlier formulation of the CPD model<sup>45</sup> showed good agreement with the temperature dependence and total volatiles yields measured by Gibbins-Matham and Kandiyoti.<sup>72</sup> Since the crosslinking rate affects the total yield as a function of heating rate, these data were used to help select values of  $E_{cross}$  for the improved CPD model. Comparisons of CPD predictions with these data using the three different values of  $E_{cross}$ , are shown in Fig. 14. Chemical structure parameters for these predictions are derived from the tar and total volatiles yields at 1000 K/s with 30 s hold at 973 K (i.e., values for  $\xi_o$  were adjusted to fit this data point for each value of  $E_{cross}$ ), since no NMR data regarding chemical structure are available for this size-classified coal. The

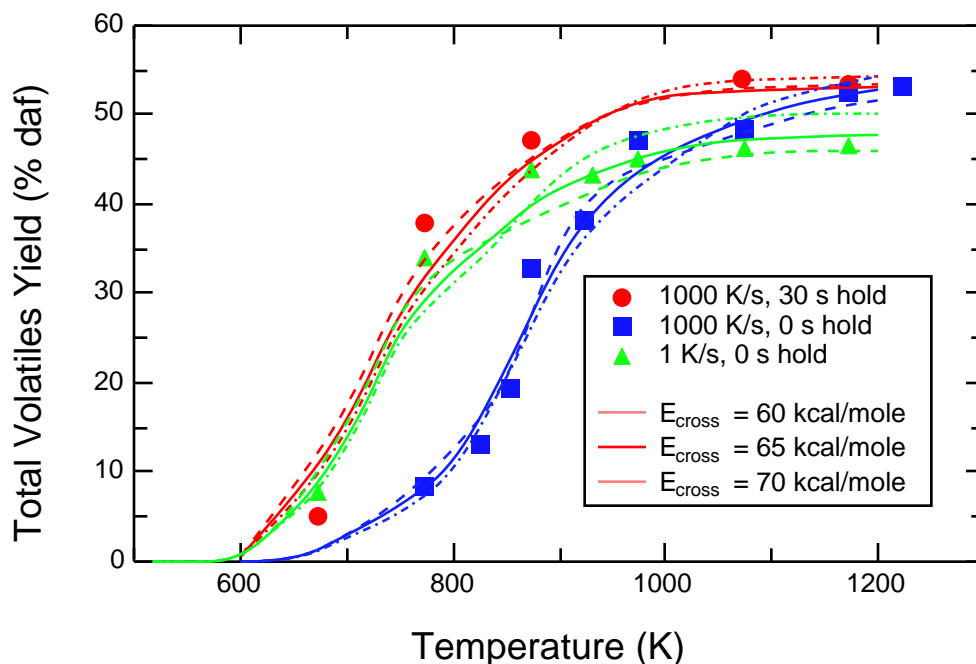


Figure 14. CPD model predictions of total volatiles yields (curves) with different values of  $E_{cross}$  compared with the heated grid data (points) of Gibbins-Matham and Kandiyoti<sup>72</sup> for a Pittsburgh No. 8 coal at different heating rates.

predictions show only a slight sensitivity to the value for  $E_{cross}$ . For example, in the 1000 K/s case with 0 s hold time, predicted total yields at 1200 K range from 50 to 53%. The predictions of total volatiles yields using  $E_{cross} = 70$  kcal/mol at 1 K/s are approximately 5% higher than the data at high temperatures (above 900 K). The value of  $E_{cross}$  of 65 kcal/mol seems to give slightly better agreement with the data in these three cases than the other two values. The relative insensitivity of the predictions to the value of  $E_{cross}$  is most likely due to the moderate temperatures (1200 K maximum) in these heated grid experiments, which limits the crosslinking rate.

Pyridine Extract Data. Fong and coworkers<sup>66</sup> measured the pyridine extract yields from chars produced during devolatilization experiments as a function of residence time on a heated screen at heating rates of  $\sim 500$  K/s. The extract yield is related to the amount of finite material (metaplast) in the char at any time. Approximately 25% of the parent bituminous coal was extracted with pyridine, and up to 65% of the parent coal appeared as extract yield during pyrolysis. However, after completion of pyrolysis, extract yields of 0% were measured.

Only qualitative comparisons of CPD model predictions can be made with the data from Fong, et al.<sup>66</sup> because pyridine extracts colloidal material (with molecular weights of several million amu) as well as metaplast that may never vaporize at typical pyrolysis conditions. The experimental extraction procedure was performed at the boiling point of pyridine (388.5 K), which may also have broken some of the weak bonds in the coal and chars. Extraction experiments performed with other solvents, such as tetrahydrofuran (THF), typically give lower extract yields ( $\sim 10\%$  or less). In addition, the mass release predicted by the CPD model occurs at residence times 10% earlier than measured by Fong and coworkers. The particle temperature histories determined in this experiment may be subject to well-known biases that commonly occur in heated-screen temperature measurements.<sup>70-74</sup> The mass release predicted by the CPD model agrees with experimental data at rapid heating rates where particle temperatures have been measured optically<sup>5,45,71</sup> and with data at low heating rates (1 K/s), as explained above.

The predicted amounts of metaplast for the Fong experiment (case D in his experiment) with a heating rate of 640 K/s and a final temperature of 1018 K are shown in Fig. 15 as a function of residence time for different values of  $E_{cross}$ , along with the pyridine extract yield data. The chemical structure and rate parameters used in these predictions are identical to those used in the predictions described in the previous section for the data of Gibbins-Matham and Kandiyoti.<sup>72</sup> The predictions show production and depletion of metaplast in the same time period that the increase in pyridine extracts occurs. As mentioned above, the predicted amount of metaplast is not expected to agree because pyridine extracts contain significant amounts of colloidal dispersions. The predictions with  $E_{cross}$  equal to 60 and 65 kcal/mol are in qualitative agreement with the residence times of the peak in the extract yield data. The prediction using  $E_{cross} = 70$  kcal/mol exhibits a long tail in the final stages of metaplast depletion (residence times between 1 and 1.5 seconds), whereas a rapid depletion of the extract yields are observed at a residence time of 1.1 seconds. The best agreement between CPD model calculations and the pyridine extract data is achieved using  $E_{cross} = 65$  kcal/mol.

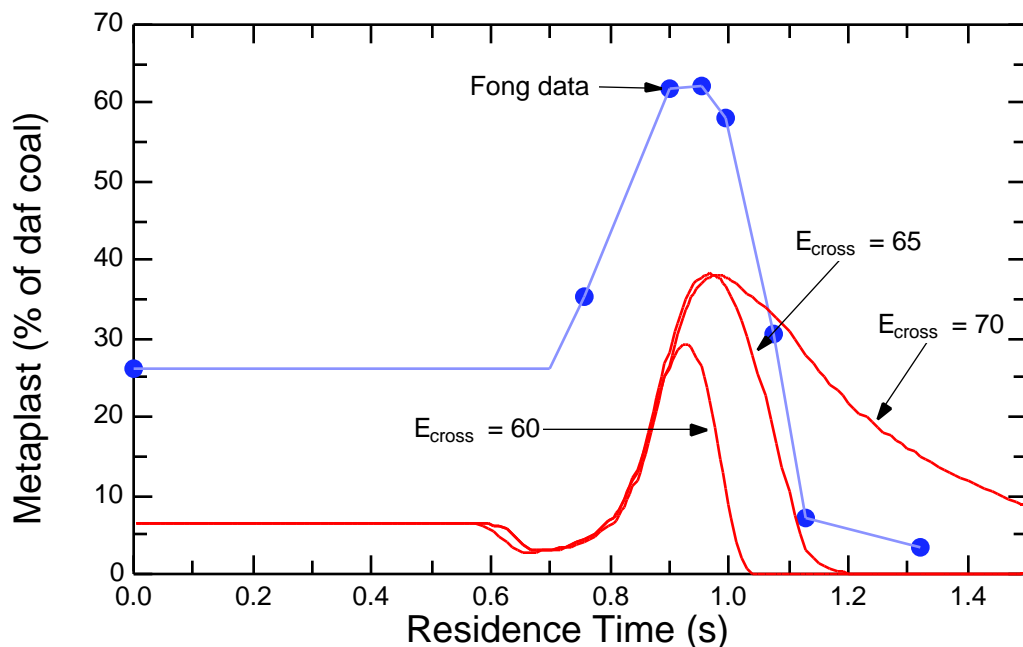


Figure 15. CPD model predictions (solid curves) of the amount of metaplast in a char particle derived from a Pittsburgh No. 8 coal, compared with pyridine extract data (points and dashed line) from a heated grid experiment.<sup>66</sup> In both the experiment and the calculations, the heating rate is 640 K/s, with a final holding temperature of 1018 K.

NMR Data. Previous measurements of the chemical structure of char particles sampled as a function of residence time in an entrained flow reactor at Sandia identify quantitatively the number of bridges and loops between aromatic clusters.<sup>29,31</sup> The number of bridges and loops per cluster is a quantitative indication of the extent of crosslinking in the solid material. For an Illinois No. 6 bituminous coal, the number of bridges and loops per cluster was shown to increase in the late stages of devolatilization, after the tar was released.<sup>29,31</sup> For a North Dakota Beulah Zap lignite, the number of bridges and loops per cluster increased early in the devolatilization process.<sup>31</sup> In the CPD model, the amount of metaplast that has been reattached to the infinite char matrix is calculated, providing a direct measure of the extent of crosslinking. Model calculations of the amount of reattached metaplast are therefore compared with the number of bridges and loops per cluster determined from NMR analyses of char samples. All input chemical structure parameters used in the CPD model for this coal are taken directly from the NMR data. Heating rates in these experiments are approximately  $10^4$  K/s, with a maximum gas temperature of 1250 K and a maximum particle temperature of 1200 K. The actual particle temperature history is determined from measurements of the size, temperature, and velocity of individual particles at different residence times in the entrained flow reactor.<sup>70,71</sup> As shown in Fig. 16 for an Illinois No. 6 bituminous coal, the model predicts that the amount of reattached metaplast remains constant until the late stages of mass release, and then increases rapidly, which agrees qualitatively with the extent of mass release at which the measured increase in the number of bridges and loops per cluster is observed. The prediction with  $E_{cross}$  equal to 70 kcal/mol shows the latest rise in the

amount of reattached metaplast, which agrees better with the NMR data than the predictions using the two lower values of  $E_{cross}$ . The uncertainties involved in these NMR data are sufficiently large, however, that only  $E_{cross} = 60$  kcal/mol can be considered to be an unlikely value.

Based on the comparisons with (i) pyridine extract data, (ii) total volatiles yields as a function of heating rate, and (iii) NMR determinations, a value of  $E_{cross} = 65$  kcal/mol was selected for use in the CPD model. All calculations presented in the remainder of this paper use  $E_{cross} = 65$  kcal/mol.

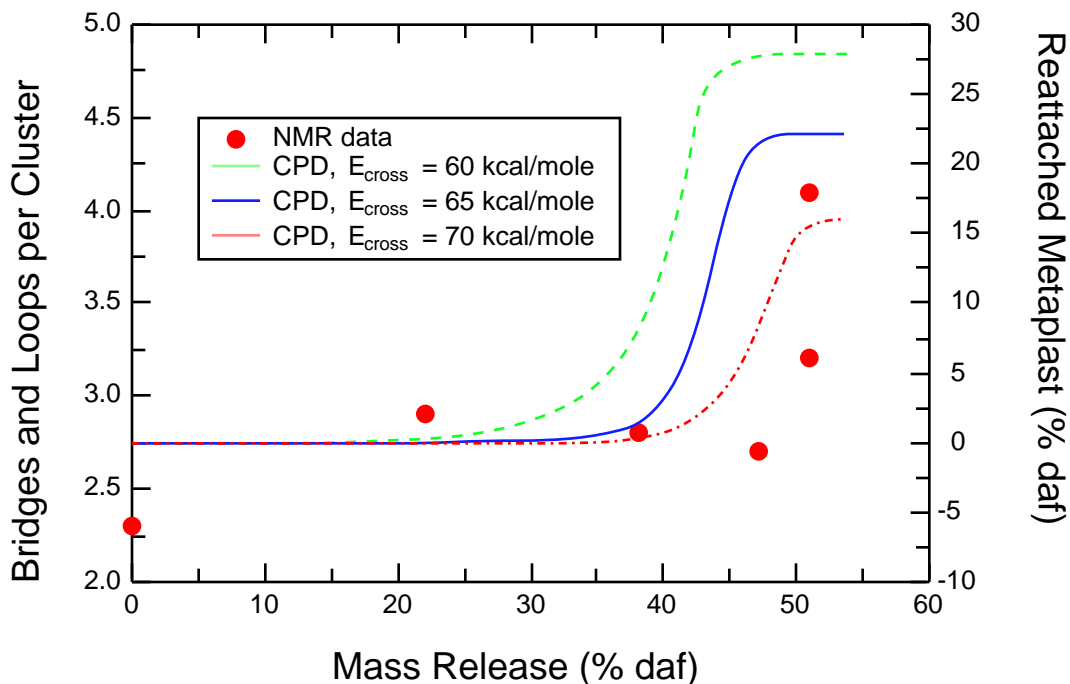


Figure 16. CPD model predictions (with different values of  $E_{cross}$ ) of the amount of reattachment of metaplast in a char derived from an Illinois No. 6 coal, compared with NMR data from an entrained flow reactor.<sup>29</sup>

**c. Chemical Structure Parameters.** The pyrolysis behavior of different coals, including product yields and release rates, is directly a function of the chemical structure of the coal. Ideally, all of the input parameters for a coal pyrolysis model should be determined from measurements of the elemental composition and chemical structure as a function of coal type. It is quite possible that sophisticated devolatilization models may be able to fit tar and gas yields, and even molecular weights, based on physically unrealistic values of chemical structure parameters. These models often have enough adjustable parameters that the physical interpretation of individual parameters becomes difficult, although in all cases "the model agrees well with the data." Such was the case with earlier formulations of the CPD model; input parameters were determined from curve-fits of tar and total volatiles yields, even though the processes of vapor-liquid equilibrium and crosslinking were not treated.<sup>6,45</sup> In the present formulation of the CPD model, five parameters

describe the chemical structure of each coal; (i) the coordination number,  $\langle +1 \rangle$ , (ii) the initial number of intact labile bridges  $\xi_o$ ; (iii) the initial number of char bridges  $c_o$ ; (iv) the hypothetical ultimate gas yield  $f_{gas}$ ; and (v) the average molecular weight of an aromatic cluster  $m_a$  (this parameter was simply set to 120 amu in the original treatment of the CPD model). The approach taken here is to take the input parameters in the CPD model directly from the NMR determinations of chemical structure, which drastically reduces the number of adjustable parameters in the model.

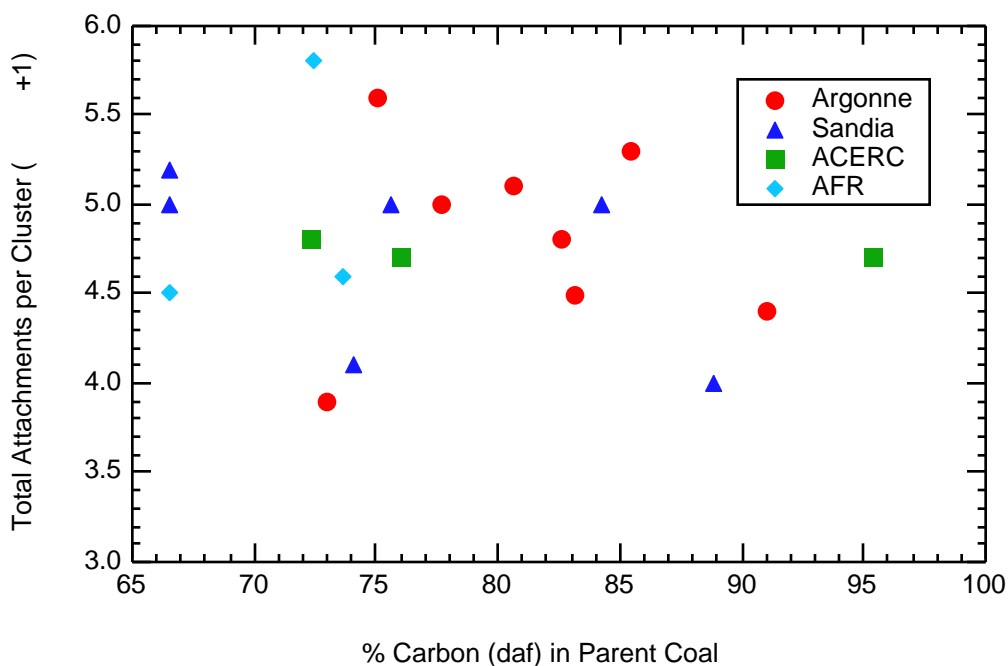


Figure 17. Total number of attachments per aromatic cluster ( $\langle +1 \rangle$ ) determined from  $^{13}\text{C}$  NMR analyses. NMR data are for coals from the Argonne premium sample bank<sup>75,76</sup> from AFR,<sup>5</sup> and from the Penn State sample bank examined at Sandia<sup>29,31,77</sup> and at BYU (ACERC).<sup>78</sup>

The coordination number ( $\langle +1 \rangle$ ) is taken directly from  $^{13}\text{C}$  NMR measurements of the parent coals using techniques described by Solum and coworkers.<sup>75</sup> Since the coordination number is defined as the total number of attachments per cluster, it accounts for side chains as well as labile and char bridges. Measured values of the coordination number range from 3.9 to 5.8, but show no systematic variation with coal rank, as shown in Fig. 17 for sixteen coals: the 8 Argonne premium coals;<sup>76</sup> 5 research coals used at Sandia National Laboratories;<sup>77</sup> 3 research coals used at Advanced Fuel Research (AFR);<sup>5</sup> and 3 coals from the ACERC suite.<sup>78</sup> Relevant chemical structure data for these coals, using techniques discussed by Solum and coworkers,<sup>33,75</sup> are shown in Table 3. The highest values of the coordination number occur for the Rosebud subbituminous coal from AFR and for the Wyodak coal from the Argonne premium sample bank. The Rosebud subbituminous coal sample analyzed by NMR spectroscopy was unfortunately subjected to oxidation over long times at room temperatures (weathering), which may have caused structural changes in the coal.

**Table 3**  
**Chemical Structure Parameters from  $^{13}\text{C}$  NMR for 19 Coals**

Coal Type	%C (daf)	$M_{\text{clust}}$	$m$	$P_o$	$f_a'$	AC/CI	+1
Zap (AR)	72.9	277	40	0.63	0.55	9	3.9
Wyodak (AR)	75.0	410	42	0.55	0.55	14	5.6
Utah (AR)	80.7	359	36	0.49	0.61	15	5.1
Ill6 (AR)	77.7	316	27	0.63	0.72	15	5.0
Pitt8 (AR)	83.2	294	24	0.62	0.70	15	4.5
Stockton (AR)	82.6	275	20	0.69	0.75	14	4.8
Freeport (AR)	85.5	302	17	0.67	0.81	18	5.3
Pocahontas (AR)	91.1	299	14	0.74	0.86	20	4.4
Zap (Sandia)	66.6	410	51	0.59	0.57	14	5.2
Zap (Sandia, repeat)	66.6	440	52	0.48	0.57	13	5.0
Blue (Sandia)	75.6	410	47	0.42	0.53	14	5.0
Ill6 (Sandia)	74.1	270	34	0.56	0.67	11	4.1
Pitt8 (Sandia)	84.2	356	34	0.45	0.60	15	5.0
Poc (Sandia)	88.8	316	18	0.70	0.77	18	4.0
Zap (AFR)	66.5	339	46	0.63	0.58	11	4.5
Rose (AFR)	72.4	459	48	0.57	0.53	15	5.8
Ill6 (AFR)	73.6	267	29	0.61	0.67	11	4.6
1443 (lig,ACERC)	72.3	297	36	0.59	0.56	10	4.8
1488 (sub,ACERC)	76.0	310	37	0.54	0.56	11	4.7
1468 (anth,ACERC)	95.4	656	12	0.89	0.94	49	4.7

AR refers to 8 coals from the Argonne premium sample bank;<sup>75,76</sup> Sandia refers to 5 coals examined at Sandia National Laboratories by Fletcher;<sup>77</sup> AFR refers to 3 coals examined by Serio, et al.<sup>5</sup> at Advanced Fuel Research (AFR); and ACERC refers to three coals examined from the Advanced Combustion Engineering Research Center (ACERC) at BYU and the University of Utah.<sup>78</sup>

The corresponding number for the Wyodak subbituminous coal, which is similar to the Rosebud coal, is 5.6. This may indicate a peculiar feature of subbituminous coals which is not completely understood at present. The coordination number has been shown to stay relatively constant in coal chars during devolatilization.<sup>29,31</sup> The distribution of attachments between side chains versus the bridges and loops per cluster, however, does change as a function of the extent of devolatilization, dependent on coal type.<sup>29,31</sup> The coordination number ( $\bar{p} + 1$ ) can be used to calculate the number of intact bridges per cluster ( $\bar{p}$ ) used by Solomon<sup>68,79</sup> as follows:  $\bar{p} = p(\bar{p} + 1)/2$ . The value of  $\bar{p}$ , measuring the number of intact bridges to clusters, is greater than 2 but less than the value of 4 to 5 for the coordination number ( $\bar{p} + 1$ ), since the coordination number accounts for side chains as well as bridges.

The population of intact bridges in the parent coal ( $p_o$ ) is also measured by  $^{13}\text{C}$  NMR, and is used as an input parameter in the CPD model, noting that  $p_o = \xi_o + c_o$ . The value of  $p_o$  therefore sets an upper bound to the number of labile bridges  $\xi_o$  in the parent coal, while  $c_o$  determines the actual fraction of the total bridges that are stable at temperatures typical of devolatilization. There seems to be no consistent variation in the measured value of  $p_o$  as a function of coal rank, as shown in Fig. 18, except for the fact that the anthracite has more intact bridges than the other coals. The scatter in these data is interpreted as diversity in coals of similar rank, and indicates more diversity

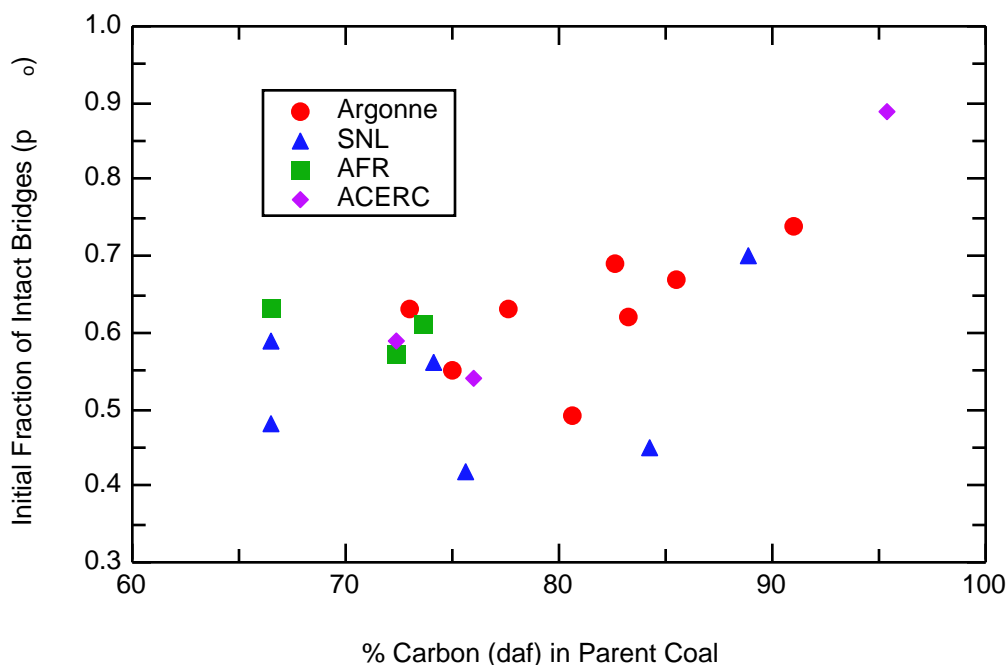


Figure 18. Initial fraction of intact bridges  $p_o$  determined from  $^{13}\text{C}$  NMR analyses. NMR data are for coals from the Argonne premium sample bank<sup>75,76</sup> from AFR,<sup>5</sup> and from the Penn State sample bank examined at Sandia<sup>29,31,77</sup> and at BYU (ACERC).<sup>78</sup>

among low rank coals than high rank coals. The value of  $c_o$  is related to the concentration of stable bridges between clusters, such as bi-aryl and aryl-ether linkages, particularly in the high rank coals. There is currently no method to measure this quantity, and  $c_o$  is determined empirically by comparing CPD model predictions with measured tar yields. In low rank coals (particularly lignites),  $c_o$  is used to approximate the early crosslinking that occurs. The introduction of a progressive crosslinking mechanism into the CPD formulation is the subject of ongoing research, and will eliminate the need to specify  $c_o$  for low rank coals.

The value of  $f_{gas}$  is related to the molecular weight of labile bridges ( $m_b$ ), the molecular weight of the aromatic part of the cluster ( $m_a$ ), the initial char bridge population ( $c_o$ ), and the coordination number ( $+1$ ) in Eq. 41. Equation 41 can therefore be rearranged to provide an expression for  $f_{gas}$  in terms of  $m_b$ , as follows:

$$f_{gas} = \frac{m_b (+1)(1 - c_o)}{[2 m_a + m_b (+1)(1 - c_o)]} \quad (62)$$

The average molecular weight of a labile bridge in the CPD model is twice the molecular weight of a side chain ( $m_b = 2m$ ). The value of  $m$  can be estimated from the  $^{13}\text{C}$  NMR data by subtracting the mass of the aromatic material from the total cluster molecular weight and dividing by the number of attachments per cluster, as follows:

$$m = \frac{M_{clust} - C_{clust} M_C}{+1} \quad (63)$$

In the NMR estimates, the high rank coals have low side chain molecular weights compared to the low rank coals, as shown in Fig. 19. This means that the Pocahontas coal contains a large number of intact bridges between aromatic clusters that are smaller than bridges observed in lower rank coals. The low rank coals contain approximately the same number of bridges per cluster, but the molecular weight of each bridge is higher. These trends correspond to measured aromaticities as a function of coal rank; high rank coals exhibit higher carbon aromaticities (and hence less aliphatic carbon) than low rank coals. The larger aliphatic bridges in the low rank coals are sometimes referred to as polymethylenes.<sup>79</sup> The NMR data are consistent with the observation that more aliphatic  $-\text{CH}_2-$  (polymethylene) is seen in FTIR spectra of low rank coal tars than in high rank coal tars.<sup>21</sup>

Realistically, an unspecified fraction of tightly-bound  $-\text{methyl}$  groups remain attached the aromatic unit at typical devolatilization temperatures. These  $-\text{methyl}$  groups are counted in the NMR measurements as side chains, but should be considered as part of the aromatic cluster in the CPD model, since they are not released during devolatilization. The fraction of tightly-bound side chains may be a significant quantity in high rank coals, such as the low volatile bituminous Pocahontas coal, where side chain molecular weights are small to begin with. Good agreement with gas yield data from Pocahontas coal was achieved when the side chain molecular weight used in the CPD model was reduced by 7 amu from the NMR measurements ( $m = 14$  as measured by NMR, so  $m' = 7$  in the CPD model for this coal). This factor of 7 amu reduction in the NMR-measured value of  $m$  was also used for all other coals; this factor becomes less important for

lower rank coals because the  $m$  is larger, reaching 52 amu for the Zap lignite from the PETC suite (PSOC-1507D).

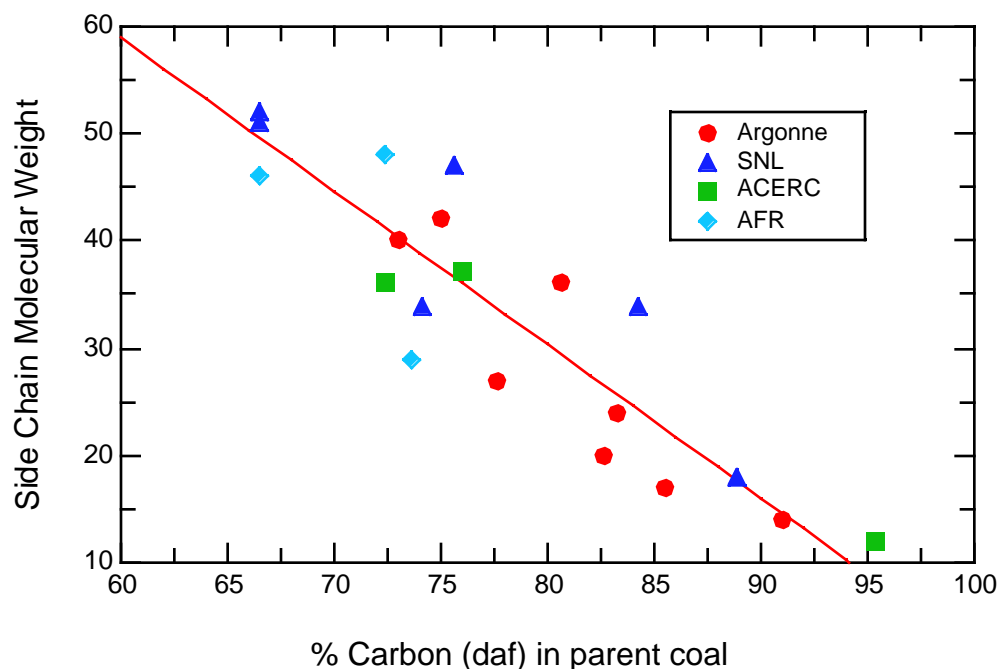


Figure 19. Measured molecular weights per side chain  $m$  determined from  $^{13}\text{C}$  NMR analyses. NMR data are for coals from the Argonne premium sample bank<sup>75,76</sup> from AFR,<sup>5</sup> and from the Penn State sample bank examined at Sandia<sup>29,31,77</sup> and at BYU (ACERC).<sup>78</sup> The line represents a correlation of the data.

The average molecular weight of an aromatic cluster ( $M_{clust}$ , as measured by Solum and coworkers<sup>75</sup>) consists of contributions by aromatic and aliphatic moieties. The molecular weight of each fragment size bin ( $m_{frag,n}$ ) in the CPD model is calculated from Eq. 32.<sup>6</sup> This equation is a nonlinear function of the number of aromatic clusters per fragment ( $n$ ), the number of intact bridges ( $p = \ell + c$ ), and the number of side chains ( $m$ ). The molecular weight of a dimer is therefore not simply twice the molecular weight of a monomer, etc. The average molecular weight of an aromatic cluster, including the side chains and half of the bridges, has also been estimated by Solum, et al.<sup>75</sup> using NMR measurements of coal structure. The molecular weight per cluster is calculated from the ratio of the number of aromatic carbons per cluster to the carbon aromaticity, as follows:

$$M_{clust} = \frac{C_{clust} M_C}{f_a' x_C} \quad (64)$$

where  $M_{clust}$  is the molecular weight per cluster,  $C_{clust}$  is the number of aromatic carbons per cluster,  $M_C$  is the molecular weight of carbon (12 amu),  $f_a'$  is the carbon aromaticity, and  $x_C$  is the

percentage of carbon in the coal (daf basis). The number of aromatic carbons per cluster increases uniformly with rank, as shown in Fig. 20. However, the NMR determinations of cluster molecular weight show no such clear trend as a function of coal rank, due to diversity in chemical structure; only a slight trend is observed that  $M_{clust}$  decreases slightly as rank increases, as shown in Fig. 21.

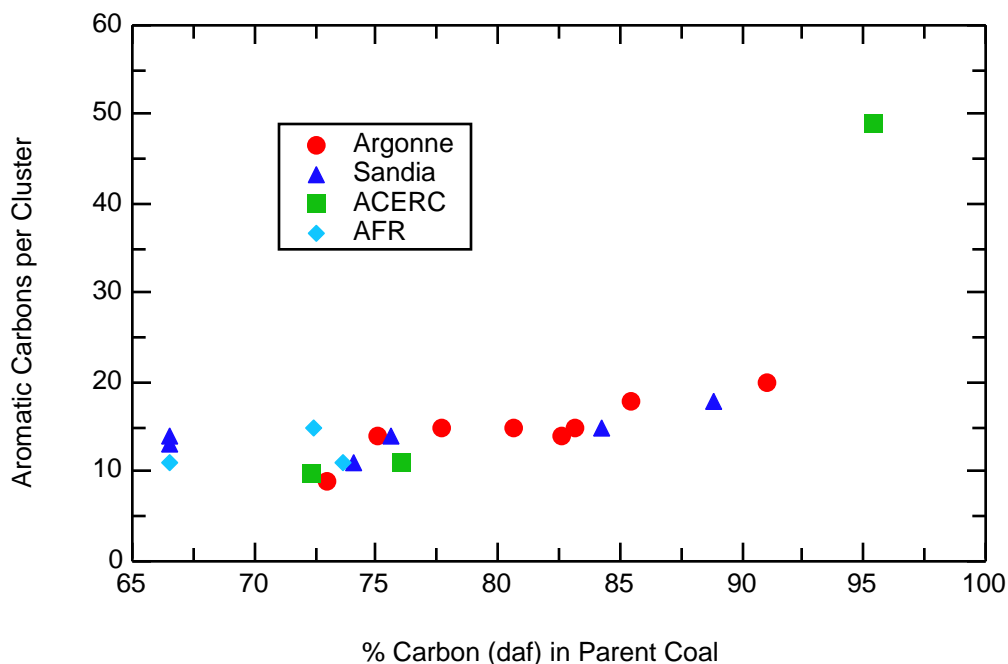


Figure 20.  $^{13}\text{C}$  NMR determinations of the average number of aromatic carbons per cluster as a function of the carbon content of the parent coal. NMR data are for coals from the Argonne premium sample bank<sup>75,76</sup> from AFR,<sup>5</sup> and from the Penn State sample bank examined at Sandia<sup>29,31,77</sup> and at BYU (ACERC).<sup>78</sup>

Knowing the molecular weight per cluster  $M_{clust}$ , the side chain molecular weight  $m$ , and the coordination number  $+1$ , the average molecular weight of the aromatic part of the cluster ( $m_a$ ) is determined in the CPD model by rearranging Eq. 63, as follows:

$$m_a = M_{clust} - m (+1) \quad (65)$$

This equation assures that the mass associated with  $-$ carbons is assigned to  $m_a$  when the measured value of  $m$  is reduced by 7 amu, as described above. Equation 65 assures that the molecular weight of a monomer fragment, as predicted by Eq. 32 with  $n = 1$ , will be equal to the cluster molecular weight  $M_{clust}$  from the NMR data.

The extensive use of NMR data for input parameters limits the amount of curve-fitting that is possible with the CPD model, and calculations become true predictions rather than empirical interpolations. As discussed above, the only adjustable coal structure parameter is the initial

population of char bridges  $c_o$ , which in effect limits the tar production from the labile bridges. This empiricism for low rank coals will be eliminated by the introduction of a progressive crosslinking mechanism in the CPD model, as discussed by Solomon and coworkers.<sup>79</sup>

The tar yields predicted by the CPD model are limited principally by the values of the coordination number  $+1$  and the initial bridge population  $p_o$ . The gas yield is principally affected by the value of  $f_{gas}$ , which is calculated directly from the average molecular weight per side chain  $m$  determined in the NMR measurements. The value of  $c_o$  limits the tar yield in the low rank coals (approximating early crosslinking) and in the high rank coals (due to finite populations of char bridges thought to exist in the parent coal matrix). The CPD calculations of tar and total volatiles yields for the high volatile bituminous coals, with  $c_o = 0$ , become true predictions based on NMR parameters. Only one coal-dependent parameter is currently used in the CPD calculations for the low or high rank coals, meaning that the total volatiles yield is a true prediction while the calculate tar yield is affected by  $c_o$ .

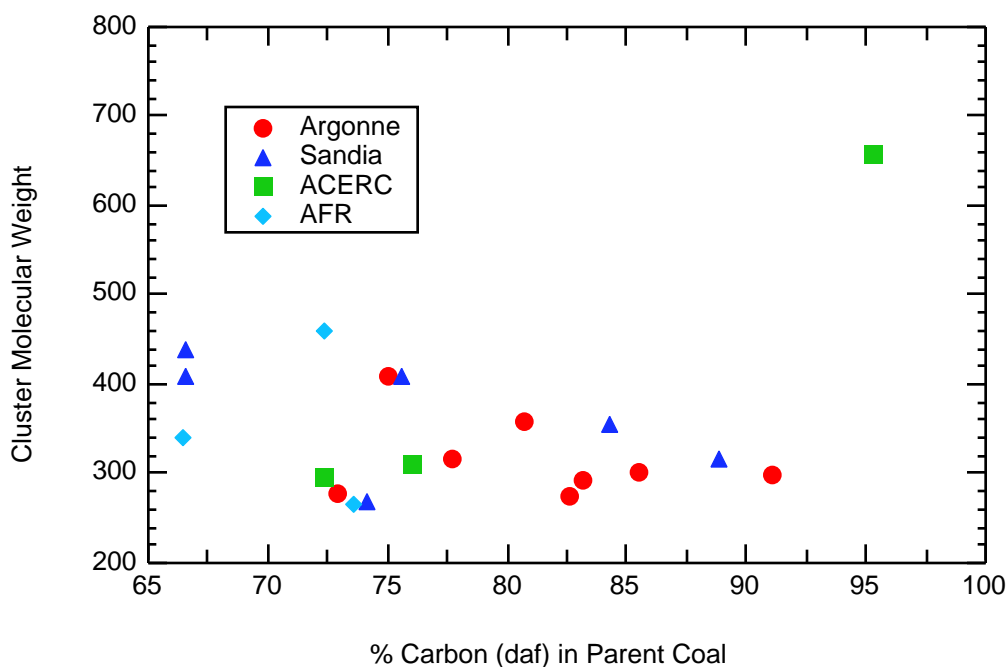


Figure 21. Measured average molecular weights per aromatic cluster  $M_{clust}$  determined from  $^{13}\text{C}$  NMR analyses. NMR data are for coals from the Argonne premium sample bank<sup>75,76</sup> from AFR,<sup>5</sup> and from the Penn State sample bank examined at Sandia<sup>29,31,77</sup> and at BYU (ACERC).<sup>78</sup>

## V. Comparison with Data

**a. Tar and Total Volatiles Yields.** Since coal-dependent chemical structure parameters for the CPD model are taken directly from NMR data, with only one adjustable parameter as explained above, predictions of tar and total volatiles yields are compared with measured yields in order to evaluate the model. Predicted tar molecular weights are also compared with available data as part of the model evaluation. The predictions of pyrolysis behavior for the high volatile bituminous coals have no adjustable parameters, since  $c_o = 0.0$  for these coals. For example, the comparisons of CPD model predictions with bituminous coal data shown in Figs. 10 and 13 were performed with no adjustable parameters (all chemical structure parameters taken directly from NMR data), while the comparisons shown in Figs. 11 and 12 used only  $c_o$  as an adjustable parameter. This method of model evaluation is in contrast to the more common route of setting the parameters to exactly match the yields and molecular weights, and then rationalizing the coefficients based on known structure.

The predictions shown in Figs. 10 to 13 show the relationships between tar release, metaplast formation, crosslinking, and gas release. In each case, the metaplast decreases slightly during the initial stages of tar release, corresponding to the release of finite fragments present in the parent coal. This is followed by labile bridge scission, generating more finite fragments which are distributed between tar and metaplast. Labile bridge scission also generates additional side chains, and a net decrease in side chains to light gas release is not seen until the end of labile bridge scission. The mass fraction of metaplast slowly decreases to zero after tar release due to crosslinking. A significant population of side chains exists at the end of these predictions. The plots of the bridge population parameters (Figs. 10b, 11b, and 12b) account for bridges and side chains released with the tar (in a manner similar to Eq. 58), but do not account for side chains removed during the crosslinking process. However, significant side chain populations are observed in  $^{13}\text{C}$  NMR analyses of chars from the Sandia experiments,<sup>77</sup> which is consistent with CPD model predictions. The distribution of the activation energy for light gas release allows gradual release of side chains as light gas as the particle temperature is increased.

CPD model predictions of tar and total volatiles yields are compared with several sets of data in Figs. 22 and 23. The data shown here were obtained (a) at low heating rates in a TGA<sup>80</sup> for the eight Argonne premium coal samples; (b) in rapid heating experiments for three coals in a heated tube reactor;<sup>5</sup> and in a laminar flow reactor for five coals at heating rates of approximately  $10^4$  K/s.<sup>71,77</sup> The tar yields in the TGA were obtained by an FTIR technique, changing the absorbance as a function of coal type. Only the maximum tar yields reported in the rapid heating experiments are used (based on mass balances), since the tar reacts further in the hot reactor gases. The tar yields are estimated to be accurate only to within  $\pm 5\%$ , due to errors in mass balances and/or absorbance values.

The general trend shown in Fig. 22 is that the low rank coals (65 to 75% carbon) attain the same total volatiles yields as the high volatile bituminous coals (80 to 85% carbon), and then the total volatiles yields decrease for the high rank coals (>85% carbon). The tar yields are generally small for the low rank coals, reach a maximum for the high volatile bituminous coals, and then decrease for the high rank coals. However, these general trends (indicated by the curves in Fig. 22) are not

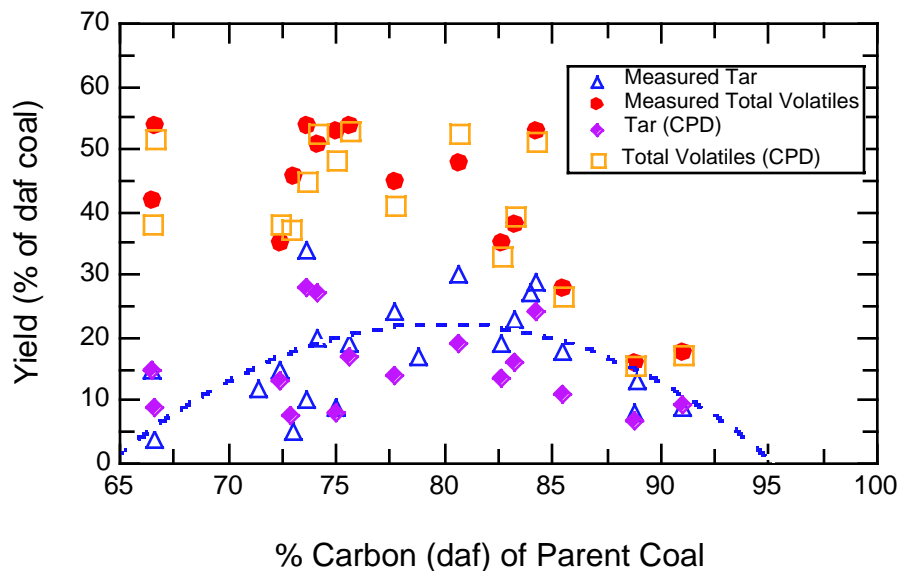


Figure 22. Comparison of predicted and measured tar and total volatiles yields for a wide range of coals. Carbon content is used to illustrate coal rank. Data are for coals from the Argonne premium sample bank,<sup>75,76</sup> from AFR,<sup>5</sup> and from the Penn State sample bank<sup>29,31,77,78</sup> for which NMR data are available.

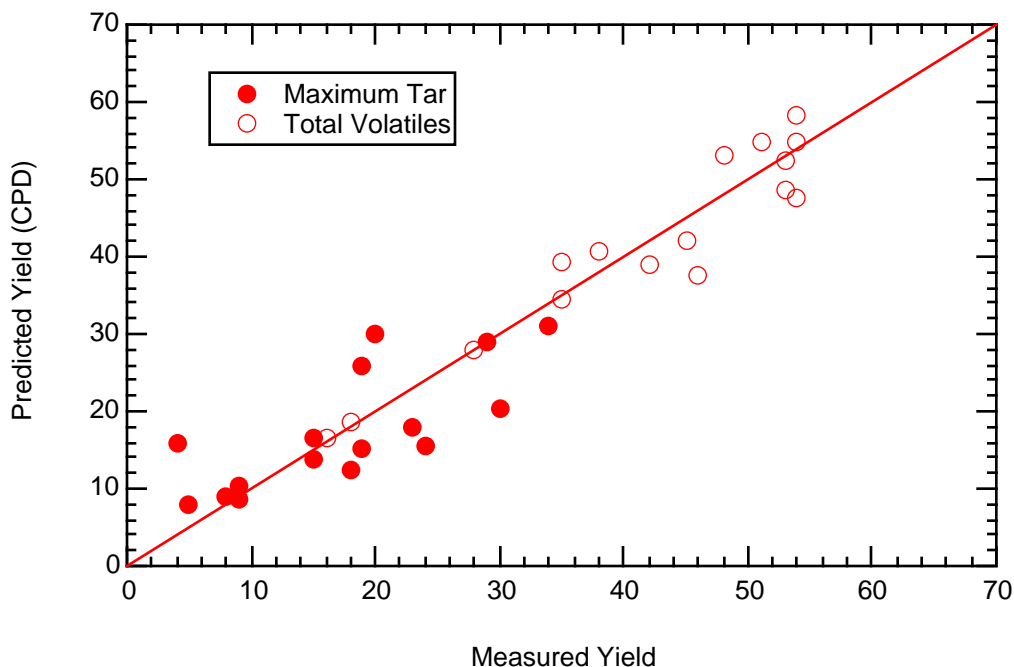


Figure 23. Comparison of predicted and measured tar and total volatiles yields for a wide range of coals. The 45° line illustrates the difference between the predicted and measured values. Data are for coals from the Argonne premium sample

universal, and there is considerable scatter in the data. The comparison of predicted tar and total volatiles yields (Fig. 23) shows that the CPD does not merely predict a trend, but rather gives quantitative agreement, even though input parameters were taken directly from NMR characterizations of coal structure. The tar yield is slightly underpredicted for high tar yields (i.e., high volatile bituminous coals), but is probably within the uncertainty in the data.

The amount of finite fragments that exist in the parent coal is a function of the initial bridge population parameters ( $\xi_o$  and  $c_o$ ) and the coordination number ( $+I$ ). At ambient temperatures, the vapor pressure of the finite fragments is much lower than the ambient pressure, and the initial finite fragments exist in the coal as metaplast. The fraction of the parent coal that exist as metaplast ( $f_{meta,o}$ ), calculated in the CPD model using the input parameters from NMR data, varies from 0.3% of the daf coal for the Pocahontas low volatile bituminous coal from the Argonne premium sample bank to 13% for the New Mexico Blue subbituminous coal (PSOC-1445D). Intermediate values of  $f_{meta,o}$  were determined for the other coals, although there is no clear distinction with coal rank. In general, the value of  $f_{meta,o}$  was lower for the Argonne coals, with a maximum of 4.9% for the Utah Blind Canyon high volatile bituminous coal. Solvents such as pyridine produce extract yields from bituminous coals as high as 25%,<sup>66,81a</sup> but contain significant amounts of colloidal dispersions.<sup>81b</sup> Other coal devolatilization models<sup>16,18</sup> use pyridine extract yields as a measure of the initial amount of metaplast. The initial fraction of metaplast in the CPD model, however, correlates with extract yields using moderate solvents with moderate contact times, such as tetrahydrofuran, where less colloidal dispersions are generally obtained than with pyridine. For instance, an extract yield of approximately 6% was obtained by soaking a Pittsburgh seam coal in tetrahydrofuran at room temperature for one hour, followed by a fifteen minute ultrasonic bath which raised the THF nearly to its boiling point.<sup>54</sup> Recent extraction experiments by Lee and coworkers,<sup>82</sup> performed in a Soxhlet apparatus for 48 hours, indicate low extract yields for Zap lignite and Pocahontas coal (2 and 1%, respectively) and moderate extract yields for high volatile Illinois No. 6 and Utah Blind Canyon coals (17 and 19%, respectively). At present, no attempt is made in the CPD model to derive input parameters from the extract yield data, since the degree of chemical interaction between the coal and the solvent is uncertain.

**b. Tar Molecular Weight.** The experimental measurement of tar molecular weight distributions is a challenging and controversial research topic. Size exclusion chromatography (SEC) and high performance liquid chromatography (HPLC) have both been used to analyze coal tars, but suffer from the difficulty in selecting calibration compounds with the same conformational geometries as exist in coal tars. Freihaut and coworkers<sup>21</sup> showed that large differences in the average tar molecular weight occur when the standard polystyrene calibration is used in SEC analyses rather than more realistic model compounds.

Another technique commonly used to determine tar molecular weights is field ionization mass spectrometry (FIMS). Relative structure differences in the tars from the eight Argonne premium coals at slow heating rates (0.05 K/s) were recently analyzed using FIMS.<sup>80</sup> Molecular weight distributions were also determined for tars from a lignite at two additional heating rates (600 K/s and 20,000 K/s). However, in the FIMS technique, it is difficult to determine the percentage of the sample that is transported through the transfer lines to the mass spectrometer; the small transfer lines may act as chromatographic columns, and absorb large and/or irregularly-shaped compounds.

As in the liquid chromatographic techniques, this method is viewed as a measure of trends in tar molecular weight distributions, and cannot be used quantitatively with great confidence.

Comparisons of trends in the calculated and measured distributions help determine if the coal structure and chemical reaction chemistry is described appropriately. In the CPD model, tar consists of a distribution of fragment sizes, and these are averaged on a mass basis. The smallest fragment size bin in the model is the average monomer molecular weight taken from NMR data, and hence represent relatively coarse size bins are used in the model. For this reason, comparisons of mass-averaged or number-averaged tar molecular weights are used to evaluate model performance. The mass-averaged tar molecular weights calculated from the CPD model are compared with SEC data from Freihaut, et al.<sup>21</sup> and FIMS data from Solomon, et al.<sup>80</sup> in Fig. 24. The carbon content is used here to approximate coal rank, in order to directly compare with the data from Freihaut and coworkers. The average tar molecular weights shown for the FIMS data were estimated by visual inspection of the spectra, and hence may be in error by approximately 50 amu. The CPD calculations were performed for rapid heating rates ( $\sim 10^3$  to  $10^4$  K/s), except for the Pocahontas lv bituminous coal. The FIMS tar data for lignite in this comparison are from the rapid heating experiment ( $2 \times 10^4$  K/s). The SEC data shown here are from Freihaut's "model compound calibration;" his data from the polystyrene calibration are 400 to 500 amu higher and are not thought to be realistic. All of the SEC data were obtained at heating rates estimated at 2000 to 5000 K/s in an entrained flow reactor where thermal radiation, rather than convection, was the dominant mode of particle heating.

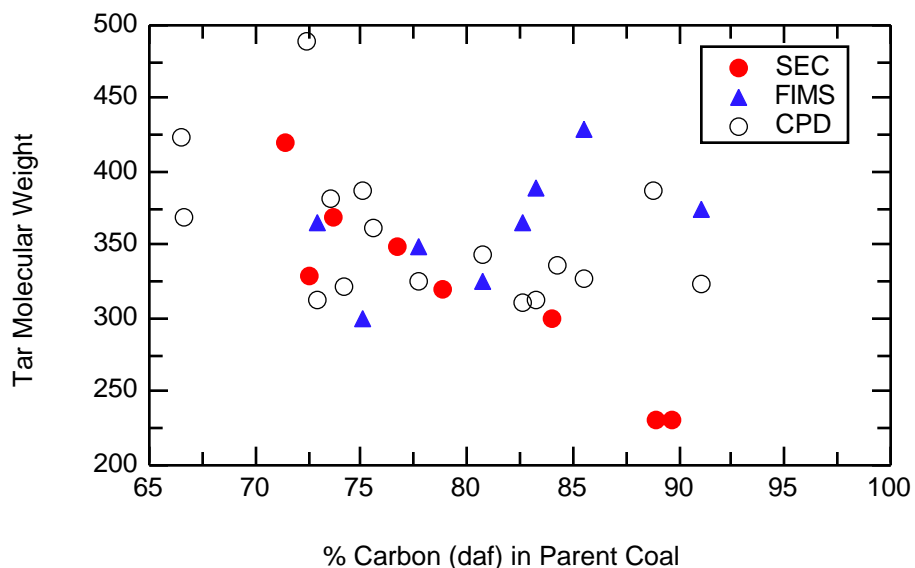


Figure 24. Mass-averaged molecular weights of tars from different coals calculated by the CPD model compared with SEC data from Freihaut, et al.<sup>21</sup> and FIMS data from Solomon, et al.<sup>67</sup> The CPD calculations were performed for rapid heating rates ( $\sim 10^4$  K/s), and the FIMS tar data for lignite are from the rapid heating experiment. The curves represent rough correlations of CPD model predictions.

The disagreement between the FIMS and the SEC tar molecular weight data is indicative of the quantitative and qualitative uncertainties in the two techniques. The high rank coal tars exhibit higher average molecular weights than the low rank coal tars in the FIMS data, while the SEC data indicate the opposite trend (low rank tars have higher average molecular weights). The CPD model predictions of average tar molecular weight show no clear trend as a function of coal rank, although a linear regression would indicate a slight decrease in tar molecular weight as rank increases. The most important conclusion from this comparison is that CPD model predictions of the average tar molecular weights from different coals, using NMR parameters as input data, are within 100 amu of both the FIMS and SEC data. Considering the uncertainty in the measurements, the overall qualitative and quantitative agreement between the predicted and measured average tar molecular weights is reasonable.

**c. Pressure Effects.** Comparisons between predictions made with the CPD model and experimental measurements performed as a function of pressure are presented in Fig. 25. Data are from heated grid experiments by Anthony<sup>83</sup> and by Suuberg and coworkers<sup>61</sup> for a Pittsburgh #8 bituminous coal; very little data other than these have been collected as a function of pressure.

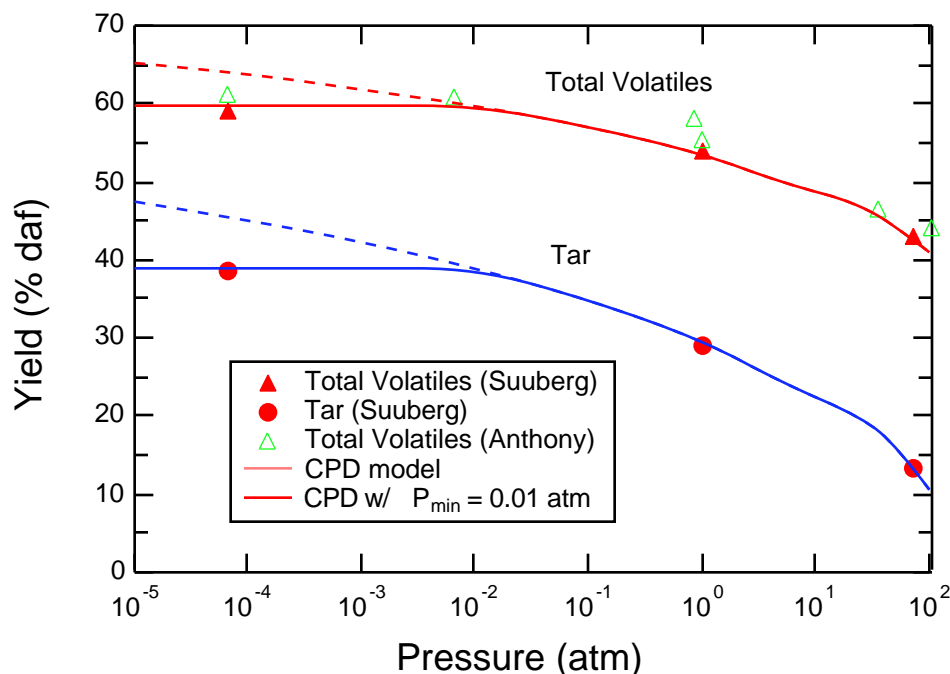


Figure 25. Comparison of CPD model predictions (curves) with pressure-dependent tar and total volatiles yield data (points) from Anthony<sup>83</sup> and Suuberg, et al.<sup>61</sup> for bituminous coals. Dashed lines represent predictions with no minimum internal particle pressure; solid lines represent predictions with a minimum internal pressure of 0.01 atm.

Particle heating rates in these experiments were approximately 1000 K/s for the Suuberg data and 700 K/s for the Anthony data, with a final temperature of 1273 K and hold times ranging from 2 to 10 s. Rate data from these early heated grid experiments are subject to questions regarding the validity of the particle temperature during the heating time.<sup>70-74</sup> The uncertainties in particle temperature during heating do not significantly affect the yield data for the long hold time experiments. Model predictions were made with a heating rate of 1000 K/s and a 5 s hold time at 1273 K using the chemical structure coefficients for a Pittsburgh No. 8 coal, with slight adjustments made to match the tar and total volatiles yield data at 1 atm.

The dashed line in Fig. 25 represents the predicted yield if there is no pressure drop inside the particle, whereas the solid line represents a minimum internal particle pressure  $P_{min}$  of 0.01 atm. A minimum internal particle pressure of 0.2 atm was used by Solomon and coworkers.<sup>18</sup> The pressure buildup inside the particle is due to volume expansion of light gases and tars during coal devolatilization. The optimum value for the parameter  $P_{min}$  in the CPD model was determined empirically from the tar yield data obtained in vacuum by Suuberg and coworkers.<sup>61</sup> The predictions made using  $P_{min} = 0.01$  atm agree quite well with the reported total volatiles and tar yields for the bituminous coal.

Model predictions of the pressure-dependent devolatilization behavior of a lignite are shown in Fig. 26, along with data from Anthony<sup>83</sup> and Suuberg.<sup>84</sup> The chemical structure coefficients used in these predictions were taken from a lignite, with adjustments in  $\xi_o$  and  $f_{gas}$ , to match the tar and total volatiles yields at 1 atm. The tar yield for this lignite is very low, hence the small effect of pressure on total yield compared to the bituminous coal. Total volatiles yields for the lignite decrease only slightly with increasing pressure in both the experimental data and the model predictions. The predicted tar yield decreases slightly with increasing pressure, but the gas yield increases to compensate, and hence the slight decrease in total volatiles yield with increased pressure.

The lignite contains a large amount of mass in the side chains and bridges, as evidenced by the relatively high average bridge molecular weight ( $m_b = 94$ ) used in the model. The number of aliphatic carbons per cluster determined by NMR analyses for lignites is twice that determined for bituminous coals.<sup>31,69,77</sup> At atmospheric pressure, the gas precursors (side chains) attached to the tar are released as tar, and can detach from the tar as light gas if the ambient gas temperature is high enough. In heated grid experiments, the gas is immediately quenched, and the gas precursors remain in the tar. At elevated pressures, more tar remains in the lignite, and the associated side chains are released as light gas. Due to the large mass in the side chains, the increased gas yield compensates for the decrease in tar yield.

## **VI. Summary**

The chemical percolation devolatilization (CPD) model discussed in this chapter includes a realistic treatment of vapor-liquid equilibrium and a crosslinking mechanism. A new, generalized vapor pressure correlation for hydrocarbons such as tar and metaplast is proposed that is based on curve-fits of vapor pressure data from coal liquids. The vapor pressure correlation compares well with pure component boiling points of hydrocarbons at pressures ranging from 0.007 atm to 10 atm and molecular weights ranging from 80 to 340 amu. This correlation is applicable to wider ranges

of pressure, temperature, and molecular weight than previous generalized correlations that were based on limited experimental data. The use of a realistic vapor pressure expression eliminates much of the empiricism used to determine coefficients for devolatilization models.

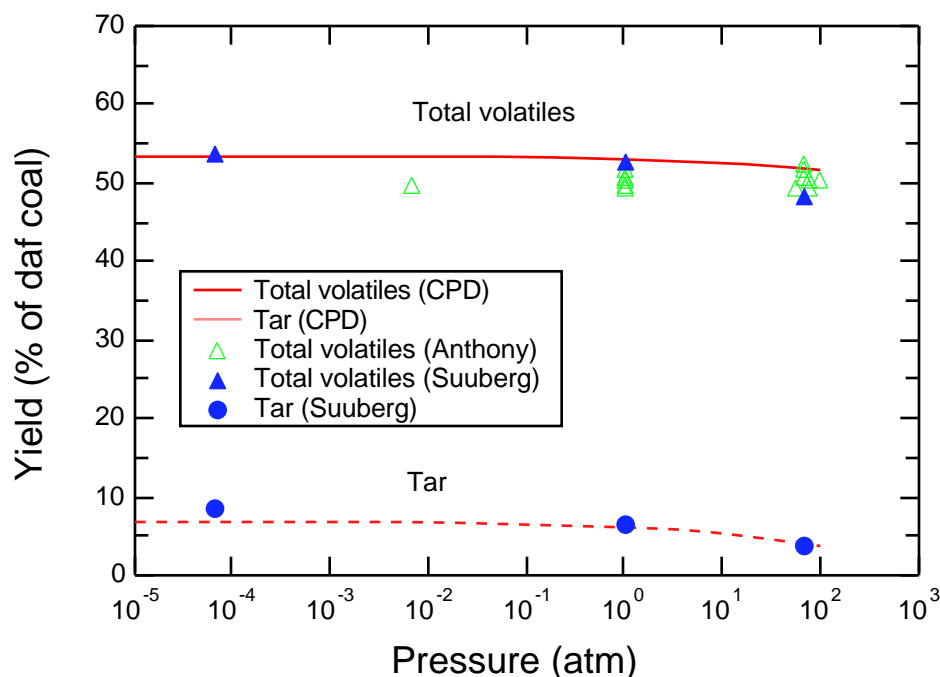


Figure 26. Comparison of CPD model predictions (curves) with pressure-dependent tar and total volatiles yield data (points) for a lignite.<sup>83,84</sup>

The crosslinking mechanism used in the CPD model permits reattachment of metaplast to the infinite char matrix. The activation energy for the crosslinking rate is selected to be 65 kcal/mol based on comparisons of CPD model predictions with: (i) measured total volatiles yields as a function of heating rate; (ii) pyridine extract data; and (iii) chemical structure data determined from NMR analyses of chars at different extents of devolatilization.

Coal-dependent input parameters for the CPD model are taken from chemical characteristics of the parent coal, wherever possible. Four of the five coal-dependent chemical structure parameters in the CPD model are taken directly from NMR analyses of the parent coal ( $+I$ ,  $M_{clust}$ ,  $m$ , and  $p_o$ ). This is a significant change in philosophy from previous treatments; these input parameters are fixed by the NMR analyses rather than used as fitting parameters. The fifth chemical structure parameter ( $c_o$ ) is 0.0 for bituminous coals and is determined from measured tar yields for low and high rank coals. In low rank coals,  $c_o$  approximates the crosslinking that occurs prior to tar release at low heating rates, as evidenced by solvent-swelling analyses<sup>67</sup> and by NMR analyses of lignites.<sup>31</sup> In high-rank coals, such as low volatile bituminous coals,  $c_o$  represents stable bridges, such as bi-aryl and aryl-ether linkages, which occur more frequently in the high rank coals than in medium and low rank coals. Identical kinetic rate parameters are used for all coals.

Predictions of the amount and characteristics of tar from sixteen different coals compare well with available data. Total yields predicted by the CPD model are also in good agreement with measured yields. The initial amounts of metaplast predicted by the CPD model for parent coals correlate roughly with 1-hour extract yields in tetrahydrofuran, rather than extract yields in pyridine. Predicted tar molecular weights roughly agree with size-exclusion chromatography (SEC) data and field ionization mass spectrometry (FIMS) data with no adjustments of the input parameters or the vapor pressure correlation.

The model quantitatively predicts the observed decrease in tar and total volatiles yields for bituminous coals as pressure is increased in heated grid experiments with long hold times, using cluster molecular weights from NMR data and the new vapor pressure correlation. As the ambient pressure increases, the vapor pressure necessary for evaporation increases, and hence lower molecular weight fractions of the metaplast are released from the coal as tar vapor. Predictions of total volatiles yields from a lignite show no increase with increasing pressure, as observed experimentally. The model shows that the lignite contains a large mass of bridge material compared to the bituminous coal, and that the decrease in tar yield with increasing pressure is compensated by an increase in gas yield for the lignite.

The CPD model includes the principal thermochemical processes involved in coal pyrolysis. The fact that many of the characteristics of tars from different types of coals can be calculated from chemical structure data for the parent coal, without artificial adjustment of vapor pressure correlations or molecular weight distributions, is encouraging. It is hoped that additional chemical structure data for coal tars and chars can be used to refine the simple mechanisms currently used in the CPD model. Attention should also be focused on molecular weight distributions, as well as on the early crosslinking that occurs in low rank coals.

### **Acknowledgements**

Discussions with Don Hardesty and Larry Baxter at Sandia are gratefully acknowledged.

## Nomenclature

$A$	pre-exponential factor for rate constant
$c$	population of char bridges, on a per bridge basis
$C_{clust}$	number of carbons per aromatic cluster
$E$	activation energy for rate constant
$f$	mass fraction, function
$f_a'$	percentage of aromatic carbon (carbon aromaticity)
$f_i$	moles of species $i$ in feed stream
$F_n$	number of $n$ -site finite fragments
$F$	moles of feed stream for flash distillation calculation
$g_1$	gas formed from side chains
$g_2$	gas formed from labile bridge stabilization to form char
$k$	kinetic rate coefficient
$K_i$	vapor-liquid equilibrium constant for species $i$ ( $K_i = y_i/x_i$ )
$l_i$	moles of species $i$ in liquid phase
$L$	moles of liquid phase for flash distillation calculation
$\ell$	population of labile bridges, on a per bridge basis
$m$	mass
$M$	molecular weight
$n$	number of aromatic clusters per finite fragment (size bin)
$p$	population of intact bridges, on a per bridge basis ( $p = \ell + c$ )
$P$	total pressure
$P_i^v$	vapor pressure of species $i$
$Q_n$	number of finite fragments on a per site basis ( $Q_n = F_n/n$ )
$r_{ba}$	ratio of mass of bridges to mass of aromatic material ( $m_b/m_a$ )
$R$	universal gas constant
$t$	time
$T$	temperature
$v_i$	moles of species $i$ in vapor phase
$V$	moles of vapor phase in flash distillation calculation
$x_C$	mass fraction of carbon (daf basis)
$x_i$	mole fraction of species $i$ in liquid phase
$y_i$	mole fraction of species $i$ in gas phase
$z_i$	mole fraction of species $i$ in feed stream
	population of side chains

$k_c/k_b$  composite rate coefficient ( $=k_c/k_b$ )  
 $+l$  number of broken bridges on the perimeter of a fragment  
 coordination number (number of attachments per cluster)

*Subscripts*

*a* aromatic  
*b* bridge  
*C* carbon  
*clust* cluster  
*cross* crosslink  
*fin* finite fragment material (detached from infinite coal matrix)  
*frag* fragment  
*gas* light gas  
*i* arbitrary species index  
*meta* metaplast  
*tar* tar  
*n* number of sites per finite fragment (monomer, dimer, trimer, etc.)  
*NMR* from nuclear magnetic resonance data on coal and char particles  
*o* initial condition (parent coal)  
 coefficient in vapor pressure correlation  
 coefficient in vapor pressure correlation  
 coefficient in vapor pressure correlation  
 side chains  
 final or infinite condition (fully pyrolyzed coal)

## References

1. Gavalas, G. R., Coal Pyrolysis, Elsevier, New York, **1982**.
2. Howard, J. B. In Chemistry of Coal Utilization; M. A. Elliott, Ed.; Wiley: New York, **1981**; p 665.
3. Solomon, P. R.; Hamblen, D. G. In Chemistry of Coal Conversion; R. H. Schlosberg, Ed.; Plenum: New York, **1985**; p 121.
4. Suuberg, E. M. In Chemistry of Coal Conversion; R. H. Schlosberg, Ed.; Plenum: New York, **1985**; p 67.
5. Serio, M. A.; Hamblen, D. G.; Markham, J. R.; Solomon, P. R. Energy and Fuels **1987**, 1, 138.
6. Grant, D. M.; Pugmire, R. J.; Fletcher, T. H.; Kerstein, A. R. Energy and Fuels **1989**, 3, 175.
7. Freihaut, J. D.; Proscia, W. M. presented at the Seventh Annual International Pittsburgh Coal Conference; Pittsburgh, Pennsylvania, September 10-14, **1990**.
8. Pitt, G. J., Fuel, **1962**, 41, 267.
9. Anthony, D. B., Howard, J. B., Hottel, H. C. and Meissner, H. P., 15th Symp (Int.) Comb., The Combustion Inst., Pittsburgh, **1975**, p 1303
10. Anthony, D.B., and Howard, J. B., A. I. Ch. E. J., **1976**, 22, 625.
11. Kobayashi, H., Howard, J. B. and Sarofim, A. F., 16th Symp. (Int.) Comb., Combustion Inst., Pittsburgh, **1977**, p. 411.
12. Niksa, S. and Kerstein, A. R., Combust. & Flame, **1986**, 66, 95.
13. Niksa, S., Combust. & Flame, **1986**, 66, 111.
14. Niksa, S., Kerstein, A. R., and Fletcher, T. H., Combust. & Flame, **1987**, 69, 221.
15. Niksa, S., AIChE Journal, **1988**, 34, 190.
16. Niksa, S.; Kerstein, A. R. Energy and Fuels**1991**, 5, 647.
17. Solomon, P. R., and Hamblen, D. G., Chemistry of Coal Conversion, R. H. Schlosberg, Ed., Plenum Press, **1985**, pp 121-251; see also a) Squire, K. R., Solomon, P. R., Carangelo, R. M., and DiTarento, M. B., Fuel, **1986**, 65, 833; b) Squire, K. R., Solomon, DiTarento, M. B., and P. R., Carangelo, R. M., A. C. S. Div. of Fuel Chem. Preprints, **1985**, 30, 386; c) Solomon, P. R., and King, H-H., Fuel, **1984**, 63, 1302; d) Solomon, P. R., Hamblen, D. G., Carangelo, R. M., Proc. International Conf on Coal Science, Sydney, Australia, **1985**, p 945; e) Solomon, P. R., and Squire, K. R., A.C.S. Div. of Fuel Chem. Preprints, **1985**, 30, 346; f) Solomon, P. R., Squire, K. R., and Carangelo, R. M., A. C. S. Div of Fuel Chem. Preprints, **1984**, 29, 10.

18. Solomon, P. R., Hamblen, D. G., Carangelo, R. M., Serio, M. A. and Desphande, G. V., *Energy and Fuel*, **1988**, 2, 405-422; see also a) Solomon, P. R., Hamblen, D. G., Carangelo, R. M., Serio, M. A. and Desphande, G. V., ACS Div. of Fuel Chem. Preprints, **1987**, 32, No.3, 83; b) Solomon, P. R., Hamblen, D. G., Desphande, G. V., and Serio, M. A., Proc. of **1987** Intern. Conf. on Coal Science, Netherlands, Eds. H. A. Moulijn, K. A. Nater, and H. A. G. Chermen, Elsevier, **1987**, p 601; .
19. Bautista, J. R., Russel, W. B., and Saville, D. A., *Ind. Engr. Chem. Fundam.*, **1986**, 25, 536.
20. Suuberg, E. M., Unger, P. E. and Larsen, J. W., *Energy & Fuels*, **1987**, 1, 305.
21. Freihaut, J. D.; Proscia, W. M.; Seery, D. J. *Energy and Fuels* **1989**, 3, 692.
22. Karr, C., Jr. (Ed), Analytical Methods for Coal and Coal Products, Academic Press, **1979**, vol III, Chaps. 46-52.
23. Chakravarti, T., Meuzelaar, H. L. C., Windig, W., Hill, G. R. and Khon, R. M., ACS Div. Fuels Preprints **1987**, 33, No. 3, p. 211.
24. Petrakis, L. and Fraissard, J. P. (Eds.) Magnetic Resonance Introduction, Advanced Topics, and Application to Fossil Energy. NATO ASI Series, Series C: Mathematical and Physical Sciences, 124, D. Reidel Pub. Co. **1983**.
25. Axelson, D. E., Solid State Nuclear Magnetic Resonance of Fossil Fuels, Multiscience Pub. Ltd. CANMET, Canadian Government Publishing Centre, Supply and Services of Canada, **1985**.
26. Gerstein, B. C. and Dybowski, C. R., Transient Techniques in NMR of Solids. An Introduction to Theory and Practice, Academic Press, **1985**, Chap 6.
27. Alemany, L. B., Grant, D. M., Pugmire, R. J. and Stock, L. N., *Fuel*, **1984**, 63, 513; Wilson, M. A., Pugmire, R. J., Karas, J., Alemany, L. B., Woolfenden, W. R., Grant, D. M. and Given, P. H., *Anal. Chem.*, **1984**, 56, 933; Wilson, M. A. and Pugmire, R. J., *Trends in Anal. Chem.*, **1984**, 3, 144; Soderquist, A., Burton, D. J., Pugmire, R. J., Beeler, A. J., Grant, D. M., Durand, B. and Huk, A. Y., *Energy & Fuels*, **1987**, 1, 50.
28. Bartuska, V. J., Maciel, G. E., Schaeffer, J. and Stejskal, E. O., *Fuel*, **1977**, 56, 354; Maciel, G. E., Bartuska, V. J., and Miknis, F. P., *Fuel*, **1979**, 58, 391; Sullivan, M. J., and Maciel, G. E., *Anal. Chem.*, **1982**, 54, 1606.
29. Fletcher, T. H.; Solum, M. S.; Grant, D. M.; Critchfield, S.; Pugmire, R. J. 23rd Symp. (Int.) Comb., Combustion Inst., Pittsburgh, **1990**, p. 1231.
30. Orendt, A. M., Solum, M. S., Sethi, N. K., Pugmire, R. J., and Grant, D. M., <sup>13</sup>C NMR Techniques for Structural Studies of Coals and Coal Chars, in Advances in Coal Spectroscopy, Plenum Press, New York, **1991**, p. 215.

31. Pugmire, R. J.; Solum, M. S.; Grant, D. M.; Critchfield, S.; Fletcher, T. H. *Fuel* **1991**, 70, 414.
32. Sethi, N. K., Pugmire, R. J. and Grant, ACS Div. of Fuel Chem., **1987**, 32, No.4, 155; D. M. Sethi, N. K., Pugmire, R. J., Facelli, J. C. and Grant, D. M., *Anal Chem*, **1988**, 60, 1574.
33. Solum, M. , Pugmire, R. J. and Grant, D. M., (**submitted for publication**), see also ACS Div. of Fuel Chem. Preprints, **1987**, 32, No.4, 273.
34. Stauffer, D., *Introduction to Percolation Theory*, Taylor and Francis, London, **1985**.
35. Fisher, M. E. and Essam, J. W., *J. Math. Phys.*, **1961**, 2, 609.
36. Kerstein, A. R. and Bug, A. L. R., *Phys. Rev. B* **1986**, 34, 1754.
37. Zallen, R., *The Physics of Amorphous Solids*, John Wiley & Sons, **1983**, Chapter 4.
38. Mohanty, K. K., Ottino, J. M. and Davis, H. T., *Chem. Eng. Sci.* **1982**, 37, 905.
39. Reyes, S. and Jensen, K. F., *Chem. Eng. Sci.* **1986**, 41, 333.
40. Niksa, S. and Kerstein, A. R., *Fuel*, **1987**, 66, 1389.
41. Kerstein, A. R. and Niksa, S., *Macromolecules*, **1987**, 20, 1811.
42. Given, P. H. *Fuel* **1960**, 39, 147.
43. Wiser, W. H. In *Proceedings of the Electric Power Research Institute Conference on Coal Catalysis Palo Alto, CA, 1973*; p 3.
44. Shinn, J. H. *Fuel* **1984**, 63, 1187.
45. Fletcher, T. H.; Kerstein, A. R.; Pugmire, A. R.; Grant, D. M. *Energy and Fuels* **1990**, 4, 54.
46. Smith, P. J. and Smoot, L. D. *Coal Combustion and Gasification*, Plenum Press, New York, **1985**.
47. Smith, P. J., Fletcher, T. H., and Smoot, L. D., *18th Int'l Symp. on Comb.* **1981**, *The Comb. Inst.* p 1285.
48. Reyes, S. and Jensen, K. F. , *Chem. Eng. Sci.* **1985**, 40, 1723.
49. Chakravarty, T.; Windig, W.; Hill, G. R.; Meuzelaar, H. L. C.; Khan, M. R. *Energy and Fuels* **1988**, 2, 400.
50. Unger, P. E.; Suuberg, E. M. ACS Div. of Fuel Chem. prepr. **1983**, 28, 278.
51. Smith, G.; Winnick, J.; Abrams, D. S.; Prausnitz, J. M. *Canadian J Chem. Eng.* **1974**, 54, 337.
52. Reid, R. C.; Prausnitz, J. M.; Sherwood, T. K. *Properties of Gases and Liquids*; Third ed.; McGraw-Hill: San Francisco, **1977**, p 196.
53. Solomon, P. R.; Hamblen, D. G.; Serio, M. A.; Yu, Z.; Charpenay, S. ACS Div. Fuel Chem. prepr. **1991**, 36, 267.
54. Unger, P. E.; Suuberg, E. M. *Fuel* **1984**, 63, 606.

55. Oh, M. S.; Peters, W. A.; Howard, J. B. *AIChE J* **1989**, 35, 775.
56. Hsu, J. Sc.D. Thesis, Department of Chemical Engineering, Massachusetts Institute of Technology, **1989**.
57. Gray, J. A.; Brady, C. J.; Cunningham, J. R.; Freedman, J. R.; Wilson, G. M. *Ind. Eng. Chem. Process Des. Dev.* **1983**, 22, 410.
58. Gray, J. A.; Holder, G. D.; Brady, C. J.; Cunningham, J. R.; Freedman, J. R.; Wilson, G. M. *Ind. Eng. Chem. Process Des. Dev.* **1985**, 24, 97.
59. Perry, R. H.; Chilton, C. H. *Chemical Engineers' Handbook*; Fifth ed.; McGraw-Hill: San Francisco, **1973**, pp 3-49.
60. Fletcher, T. H.; Hardesty, D. R. "Coal Combustion Science: Task 1, Coal Devolatilization," DOE/PETC Quarterly Progress Report for January to March, **1990**, Ed. D. R. Hardesty, Sandia Report No. SAND90-8223, available NTIS.
61. Suuberg, E. M.; Peters, W. A.; Howard, J. B. Seventeenth Symp. (Int.) on Comb.; The Combustion Institute: Pittsburgh, Pennsylvania, **1978**, p 117.
62. King, C. J. *Separation Processes*; McGraw-Hill: San Francisco, **1970**, pp 70-71, 511-512.
63. Rachford, H. H., Jr.; Rice, J. D. *Petrol. Technol.* **1952**, 4, sec. 1, p. 19; sec. 2, p. 3.
64. Gerald, C. F. *Applied Numerical Analysis*; Addison Wesley: Menlo Park, 1978, p 11.
65. Suuberg, E. M.; Unger, P. E.; Lilly, W. D. *Fuel* **1985**, 64, 956.
66. Fong, W. S.; Peters, W. A.; Howard, J. A. *Fuel* **1986**, 65, 251.
67. Solomon, M. A.; Serio, M. A.; Deshpande, G. V.; Kroo, E. *Energy and Fuels* **1990**, 4, 42.
68. Solomon, P. R., Hamblen, D. G., Yu, Z., and Serio, M. A. *Fuel* **1990**, 69, 754.
69. Fletcher, T. H.; Hardesty, D. R. "Coal Combustion Science: Task 1, Coal Devolatilization," DOE/PETC Quarterly Progress Report for June to September, **1990**, Ed. D. R. Hardesty, Sandia Report No. SAND90-8247, available NTIS.
70. Fletcher, T. H. *Combustion Science and Technology* **1989**, 63, 89.
71. Fletcher, T. H. *Combustion and Flame* **1989**, 78, 223.
72. Gibbins-Matham, J.; Kandiyoti, R. *Energy and Fuels* **1988**, 2, 505.
73. Freihaut, J. D.; Proscia, W. M. *Energy and Fuels* **1989**, 3, 625.
74. Solomon, P. R.; Serio, M. A.; Carangelo, R. M.; Markham, J. R. *Fuel* **1986**, 65, 182.
75. Solum, M. S.; Pugmire, R. J.; Grant, D. M. *Energy and Fuels* **1989**, 3, 187.
76. Vorres, K. S., "Users' Handbook for the Argonne Premium Coal Sample Bank," Argonne National Laboratory, supported by DOE contract W-31-109-ENG-38, September, **1989**. Also Vorres, K. S. *ACS Div. Fuel Chem. prepr.*, **1987** 32:4, 221.

77. Fletcher, T. H. ; Hardesty, D. R. "Compilation of Sandia Coal Devolatilization Data: Milestone Report," Contract Report for DOE's Pittsburgh Energy Technology Center, contract FWP 0709, Sandia Report No. SAND92-8209, **1992**, available NTIS.
78. Smith, K. L.; Smoot, L. D., Prog. Energy Combust. Sci., **1990** 16, 1.
79. Solomon, P. R.; Fletcher, T. H.; Pugmire, R. J. Proceedings of the Pittsburgh Coal Conference; Pittsburgh, **1990**, p 3.
80. Solomon, M. A.; Serio, M. A.; Carangelo, R. M.; Bassilakis, R.; Gravel, D.; Baillargeon, M.; Baudais, F.; Vail, G. Energy and Fuels **1990**, 4, 319.
81. (a) Berkowitz, N. Coal Science and Technology 7: The Chemistry of Coal; Elsevier: New York, **1985**, pp 40-41; (b) *ibid.*, p 283.
82. Carlson, R. E.; Critchfield, S.; Vorkink, W. P.; Dong, J.-Z.; Pugmire, R. J.; Bartle, K. D.; Lee, M. L.; Zang, Y.; Shabtai, J. *Fuel* **1991** (in press).
83. Anthony, D. B. Sc.D. Thesis, Department of Chemical Engineering, Massachusetts Institute of Technology, **1974**.
84. Suuberg, E. M. Sc.D. Thesis, Department of Chemical Engineering, Massachusetts Institute of Technology, **1977**.

## APPENDIX

**I. Fragment Statistics.** In this development the formalism of Fisher and Essam<sup>35</sup> is followed closely, and the reader is referred to this treatment for a comprehensive discussion of percolation theory. The mass fractions used in typical devolatilization work of necessity must be given on a mass or site basis while the most convenient dynamical variables are bridge variables. Fortunately, the conversion is straightforward between the expressions of Fisher and Essam given on either a per site or a per bridge basis. The Bethe pseudo lattice has a coordination number  $(z + 1)$ , and the populations of unbroken and broken bridges are  $p$  and  $(1 - p)$ , respectively. The configurational states of different bridges (broken vs. unbroken) are assumed to be statistically independent. Under these assumptions, the probability,  $F_n(p)$ , of a given site being a member of a fragment of  $n$  cluster sites with  $s$  bridges and isolated with  $z$  broken bridges is given by:

$$F_n(p) = nb_n^{site} p^s (1 - p)^z \quad (\text{A1})$$

where

$$s = (n - 1)z \quad \text{and} \quad z = n(z - 1) + 2 \quad (\text{A2})$$

The number density of  $n$ -site fragments on a per site basis then becomes,

$$Q_n(p) = F_n(p)/n = b_n^{site} p^{n-1} (1 - p)^{n(z-1)+2} \quad (\text{A3})$$

The quantity  $nb_n^{site}$  is the number of distinct fragment configurations consisting of  $n$  sites which contain a given site. Using the bridge formulation of Fisher and Essam,<sup>35</sup>  $b_n^{site}$  can be expressed as follows:

$$b_n^{site} = \frac{(z + 1)}{2} b_{n-1}^{bridge} \quad (\text{A4})$$

where the number of distinct fragments with  $s$  bridges containing a given bridge is  $sb_s^{bridge}$ . Here, the factor  $(z + 1)/2$  is used in the Bethe lattice to convert from a bridge basis to a site basis. In terms of binomial coefficients,  $b_s^{bridge}$  is given by Fisher and Essam<sup>35</sup> as follows:

$$b_s^{bridge} = \frac{2}{(s + 1)(s + z + 1)} \binom{s + z + 1}{s} \quad (\text{A5})$$

Henceforth,  $b_n^{site}$  is denoted simply as  $b_n$ . Thus, using Eq. A2 for  $s$  and  $\mu$ , Eqs. A4 and A5 give:

$$n b_n = \frac{s+1}{s+1} \binom{s+1}{s} = \frac{s+1}{n+1} \binom{n+1}{n-1} \quad (A6)$$

where the binomial coefficient is given by

$$\binom{s}{\mu} = \frac{s!}{\mu! (s-\mu)!} \quad (A7)$$

for  $s$  and  $\mu$  integers or when  $s$  and  $\mu$  are non-integer, then

$$\binom{s}{\mu} = \frac{\Gamma(s+1)}{\Gamma(\mu+1) \Gamma(s-\mu+1)} \quad (A8)$$

$\Gamma$  is the well known gamma function. The use of Eqs. A6 and A1 along with Eq. A7 or A8 gives an analytical expression for the probability of finding a fragment of size  $n$  associated with a given site on a Bethe lattice with bridge population  $p$ .

**II. Cumulative Probabilities.** Two useful summation quantities,  $B(z)$  and  $G(z)$  are defined as follows:

$$B(z) = \sum_{n=1}^{\infty} b_n z^n \quad (A9)$$

and

$$z G(z) = z \frac{B(z)}{z} = \sum_{n=1}^{\infty} n b_n z^n \quad (A10)$$

where the argument  $z$  is given by

$$z = x y^{-1} = p(1-p)^{-1} \quad (A11)$$

The differential form of Eq. A11 is useful later in integrating  $B(z)/z$  and provides a way for determining the maximum in  $z$  to be at  $p = 1/2$ . This expression is given as follows:

$$dz/dp = (1-p)(1-p)^{-2} \quad (A12)$$

Summing over Eq A1, the total fraction of sites contained in all of the finite fragments is given by,

$$F(p) = \sum_{n=1}^{\infty} F_n(p) = \sum_{n=1}^{\infty} \frac{y^n}{x^n} b_n z^n = \frac{y^2 z}{x} G(z) = y^{-1} G(z) \quad (\text{A13})$$

As shown by Fisher and Essam<sup>35</sup> both the infinite array and the finite fragments exist simultaneously above the maximum value of  $p = 1/2$ . Below this critical point only finite fragments will be found in the sample, and  $F(p)$  must equal unity. Thus,  $G(z)$  may be evaluated from eq. A13 by taking  $p < 1/2$ , which gives:

$$G(z) = \frac{1}{(1 - p^*)^{-1} + 1} \quad (\text{A14})$$

where  $p^*$  is the appropriate root of

$$z = p^*(1 - p^*)^{-1} = p(1 - p)^{-1} \quad (\text{A15})$$

Below the critical point,  $p < 1/2$ , the trivial root of  $p^* = p$  is used to obtain  $G(z)$ . Above the critical point,  $p > 1/2$ , the non-trivial root of Eq. A15 is required to evaluate  $G(z)$  and in turn  $F(p)$ . It should be noted that a given value for  $z$  may be obtained from two different values of  $p$  in the range of 0 to 1, and the value of  $p^*$  to be used in Eq. A14 must be selected to give the physically real situation. Conveniently, the appropriate physical value of  $p^*$  in the numerical solution to Eq. A15 always falls in the range  $0 < p^* < 1/2$  for values of  $p$  both above and below this critical point. Above the percolation point the expression for  $F(p)$  is no longer equal to 1 but is given by a combination of Eqs. A13 and A14 as follows:

$$F(p) = \sum_{n=1}^{\infty} F_n(p) = \left[ \frac{1 - p}{1 - p^*} \right]^{-1} = \left[ \frac{p^*}{p} \right]^{(1 - p^*) / (1 - p)} \quad (\text{A16})$$

where the latter result is obtained using Eq. A15. The fraction of sites located in the infinite array,  $R(p)$ , may now be obtained from the value of  $F(p)$ .

$$R(p) = 1 - F(p) \quad (\text{A17})$$

The configuration generating function defined in terms of  $Q_n(p)$  is given as follows:

$$K(x, y) = \sum_{n=1}^{\infty} Q_n(p) = \frac{y^2}{x} \sum_{n=1}^{\infty} b_n x^n y^{n(\alpha-1)} = \frac{y^2}{x} B(z) \quad (\text{A18})$$

where again the substitutions,  $x = p$  and  $y = (1 - p)$ , may be used. Integrating Eq. A10 using Eq. A14 for  $G(z)$  yields a value for  $B(z)$  in terms of the root  $p^*$  as follows:

$$B(z) = \frac{(\alpha + 1) - 2p^*}{2(1 - p^*)^2} - \frac{(\alpha + 1)}{2} \quad (\text{A19})$$

and from Eqs. A18 and A19 a value for  $K(p)$

$$K(p) = \left[ 1 - \left( \frac{\alpha + 1}{2} \right) p^* \right] \left[ \frac{p^*}{p} \right]^{(\alpha + 1)/(\alpha - 1)} \quad (\text{A20})$$